CHEMISTRY
AN ASIAN JOURNAL

www.chemasianj.org

Accepted Article

Title: Synthesis & Structure-Photophysics Evaluation on 2-N-Aminoquinazolines – Small-Molecule Fluorophores for Solution and Solid State

Authors: Bernhard Witulski, Miho Motoyama, Thu Hong Doan, Paulina Hibner-Kulicka, Ryo Otake, Malgorzata Lukarska, Jean-Francois Lohier, Kota Ozawa, Shinkoh Nanbu, Carole Alayrac, and Yumiko Suzuki

To be cited as: *Chem. Asian J.* 10.1002/asia.202100534

Link to VoR: https://doi.org/10.1002/asia.202100534

A Journal of

ACES
Asian Chemical Editorial Society

A sister journal of **Angewandte Chemie** and **Chemistry – A European Journal**

WILEY-VCH

10.1002/asia.202100534

WILEY-VCH

FULL PAPER

Synthesis & Structure-Photophysics Evaluation of 2-*N*-Amino-quinazolines – Small-Molecule Fluorophores for Solution and Solid State

Miho Motoyama,[a] Thu-Hong Doan,[b] Paulina Hibner-Kulicka,[b] Ryo Otake,[a] Malgorzata Lukarska,[b] Jean-Francois Lohier,[b] Kota Ozawa,[a] Shinkoh Nanbu,[a] Carole Alayrac,[b] Yumiko Suzuki,*[a] and Bernhard Witulski *[b]

[a] Prof. Dr. Y. Suzuki, Prof. Dr. Nanbu, M. Motoyama, R. Otake, K. Ozawa
Department of Life and Material Sciences, Faculty of Science and Technology, Sophia University,
7-1 Kioicho, Chiyodaku, 102-8554 Tokyo, Japan

[b] Prof. Dr. B. Witulski, Dr. T.-H. Doan, P. Hibner-Kulicka, M. Lukarska, J.-F. Lohier, Dr. C. Alayrac
Laboratoire de Chimie Moléculaire et Thio-organique, CNRS UMR 6507, ENSICAEN & UNICAEN, Normandie Univ.
6 Bvd Maréchal Juin, 14050 Caen, France
E-mail: bernhard.witulski@ensicaen.fr

Supporting information for this article is given via a link at the end of the document.

Abstract: 2-*N*-aminoquinazolines were prepared by consecutive S_NAr functionalization. X-ray structures display the nitrogen lone pair of the 2-*N*-morphilino group in conjugation with the electron deficient quinazoline core and thus representing electronic push-pull systems. 2-*N*-aminoquinazolines show a positive solvatochromism and are fluorescent in solution and in solid state with quantum yields up to 0.73. Increase in electron donor strength of the 2-amino substituent causes a red-shift of the intramolecular charge transfer (ICT) band (300-400 nm); whereas the photoluminescence emission maxima (350-450 nm) is also red-shifted significantly along with an enhancement in photoluminescence efficiency. HOMO-LUMO energies were estimated by a combination of electrochemical and photophysical methods and correlate well to those obtained by computational methods. ICT properties are theoretically attributed to an excitation to Rydberg-MO in SAC-CI method, which can be interpreted as n-π* excitation. 7-Amino-2-*N*-morpholino-4-methoxyquinazoline responds to acidic conditions with significant increases in photoluminescence intensity revealing a new turn-on/off fluorescence probe.

Introduction

Quinazolines are an important class of heterocyclic aromatic compounds providing a privileged molecular platform for medicinal chemistry and materials sciences.[1-2] The quinazoline motif is found in a broad variety of pharmaceutical active molecules possessing anti-inflammatory,[3] antitubercular,[4] antiviral,[5] antimalarial,[6] antibacterial,[7] antifungal,[8] antimutagenic,[9] antileishmanial,[10] antiobesity,[11] and particularly anticancer activities.[12] Quinazoline-based compounds are widely used in the search for new anti-cancer agents that led to several marketed drugs. Examples are gefitinib, lapatinib and erlotinib,[13] being used as single- and dual-target epidermal growth factor receptor (EGFR), as well as human epidermal growth factor receptor-2 (HER-2) drugs for the treatment of non-small-cell lung or metastatic breast cancer (Figure 1).[14] Other available quinazoline-based pharmaceuticals, which have *N*-amino functions in 2,4-position and act as α1- adrenergic receptor antagonists, are - for example - bunazosin, alfuzosin, terazosin, and prazosin.[15]

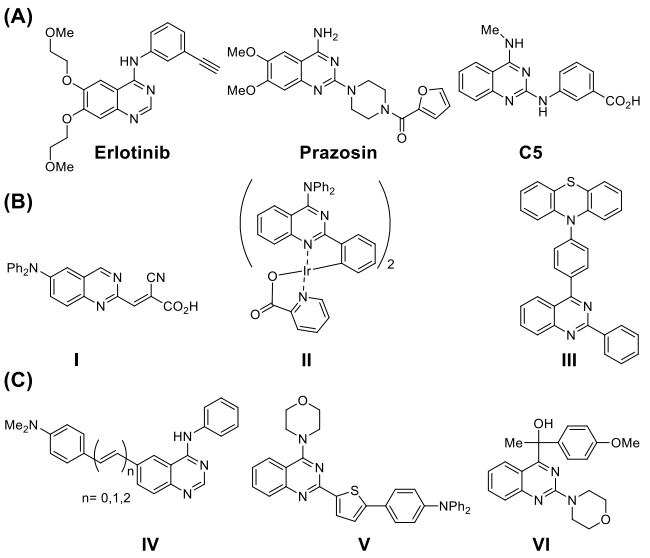

Figure 1. (**A**) Representative quinazoline-based pharmacophores & drugs, (**B**) photochromic materials used for DSSCs and OLEDs, and (**C**) small-molecule fluorescent quinazolines as molecular probes.

compounds exhibit selective CYP1A2 inhibition and might function in cancer chemoprevention.[16] Other 2,4-diaminosubstituted quinazolines have been revealed as interesting candidates for developing agents to treat Alzheimer's disease.[17] Notably, very recently the quinazoline C5 was identified as selectively binding and stabilizing an attenuator hairpin in the SARS-CoV-2 RNA genome. When C5 was linked to a RIBOTAC (ribonuclease-targeting chimera) a considerable lead for future therapeutics against SARS-CoV-2, the virus that causes COVID-19, evolved.[18]
Besides such a broad and diversified spectrum of biological activities, quinazolines have also attracted emergent interest in materials research. The electron deficient nature of the heteroaromatic core turns it to an unique molecular scaffold for the design of donor-π-spacer-acceptor chromophores,[19] low-band gap materials

10.1002/asia.202100534

for organic electronics and organic light emitting diodes (OLEDs),[20] exciplex-forming and/or dual emissive compounds,[21,22] and chemical sensors.[23] For instance, the donor-π-spacer-acceptor chromophore **I** has been used in dye sensitized solar cells (DSCCs),[24] and the quinazoline ligated iridium complex **II** was used as a yellow-red light emitting phosphorescent dopant in polymer matrixed OLEDs.[25] The quinazoline moiety is a suitable electron acceptor in thermally activated delayed fluorescence (TADF) systems for high performance OLEDs,[26] and compound **III** was used in a pure organic molecular white light-emitting OLED with dual light emission due to conformational isomerization.[22a,27]

Whereas the significance of the quinazoline molecular scaffold for pharmaceutical research is widely known, less information is available about their potential use for the development of new small-molecule fluorescent dyes. UV-vis absorption, solvatochromism and photoluminescence properties of 2,4-disubstituted aryl, arylvinyl, arylethynyl quinazolines in solution have been reported.[19a,28] Likewise, fluorescence properties of the *N*-phenyl-4-aminoquinazolines **IV** targeting the ATP-binding pocket of the ERBB family of receptor tyrosine kinases were investigated.[29] Compounds **IV** have weak to moderate fluorescence quantum yields in solution (ϕ_F = 0.17-0.37) and their emission properties are attributed to polar charge transfer excited states. Furthermore, series of 2-(thiophen-2-yl)-4-(*N*-morpholino)-quinazolines were investigated along their photophysical properties with **V** showing a solvent dependent green emission (λ_{em} (CH_3CN) = 544 nm; ϕ_F = 0.23).[30]

Recently, we reported on the fluorescent anti-cancer quinazoline **VI** as a molecular probe showing bright solvent dependent fluorescence in solution (λ_{em} (H_2O) = 460 nm; ϕ_F = 0.15; λ_{em} (hexanes) = 414 nm; ϕ_F = 0.53) that was blue shifted with emission intensity enhancement when binding to the colchicine site of β-tubulin.[31] These preliminary results indicated that 2-*N*-amino substituted quinazolines resemble a new class of small-molecule fluorophores which have - due to their underlying pharmacophore - great potential for application as molecular probes for sensing and imaging. However, less is known about the detailed photophysical properties of 2-*N*-aminoquinazolines and their derivatives, i.e. the influence of substituents on the fluorescence emission efficiency.

Here, we report on a first full investigation of the photophysical properties of a set of 2-*N*-aminoquinazolines in solution and solid state together with cyclic voltammetry and computational studies to evaluate HOMO/LUMO energy levels and charge distribution. This study aims gaining insight into fluorescence-structure-property relationship (FSPR) which will be instructive for the development of new 2-*N*-aminoquinazoline small-molecule fluorophores with unique applications.

Results and Discussion

Synthesis, Characterization, and Crystallographic Analysis

Numerous syntheses of 2-, 4-, and 2,4-disubstituted quinazolines have been reported allowing access to a broad variety of substitution pattern.[32] One of the most reliable procedures for introducing an *N*-amino group in either 2- and/or 4-position of the quinazoline core is based on readily available 2- or 4-chloro-, as well as 2,4-dichloroquinazolines and primary or secondary amines.[33]

Accordingly, a first set of quinazolines needed for our study having *N*-morpholino substituents in either 4-, 2-, or 2,4-position became available through nucleophilic aromatic substitution (S_NAr). Adding an excess of morpholine to a solution of the corresponding chloroquinazolines **1**, **3a-c**, or **5a** in 1,4-dioxane under elevated temperature gave the expected *N*-morpholinoquinazolines **2** and **4a-d** in high yield (Scheme 1). Notably, the efficiency of the S_NAr reaction at the 2-position of the quinazoline core was not affected by the kind of substituent at the 4-position. This procedure also allowed a twofold amination to give the 2,4-bis-*N*-morpholino-quinazoline **4d** in a "one-flask reaction" in 95% yield.

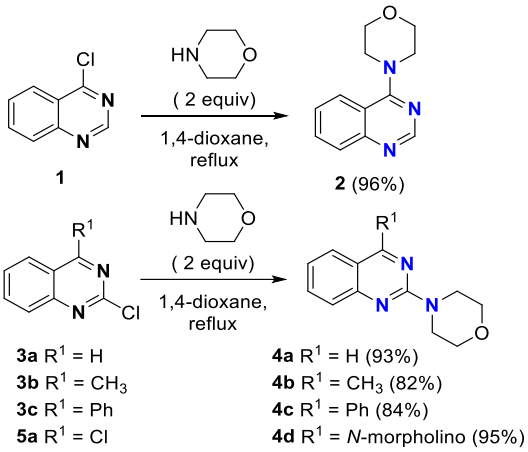

Scheme 1. Synthesis of a set of 4-, 2-, or 2,4-disubstituted quinazolines. Yield of isolated material after column chromatography on silica gel in parentheses.

A second set of fluorescent quinazolines was obtained through side-selective consecutive S_NAr reactions starting from the 2,4-dichloroquinazolines **5a-k** (Scheme 2). An initial S_NAr reaction using sodium methanolate in methanol proceeded at the more reactive 4-position of the 2,4-dichloroquinazoline core to give the 2-chloroquinazolines **6a-k** selectively (60-90% yield, Table 1). The amino function in 2-position was thereafter introduced at slightly higher reaction temperatures (up to 100 °C) through a second nucleophilic displacement of the quinazoline-2-chlorine by various amines having different sizes and nucleophilicities.[34] Notably, the less nucleophilic aziridine yielded the product **7e** in only 20% yield in a sole S_NAr reaction in 1,4-dioxane as the solvent. However, the aziridine moiety could be introduced much more efficiently into the desired 2-position by Buchwald-Hartwig arylamination:[35] With the pre-catalyst $Pd(OAc)_2$/Xantphos and Cs_2CO_3 as base the reaction of **6a** with aziridine in toluene provided the *N*-aziridine bearing quinazoline **7e** in 73% yield.[36]

Side-selective functionalizations of quinazolines were also effective for gaining access to the quinazolines **8a-d**, **9a-d**, **10** and **11** bearing respectively methoxy-, chloro- or nitro-groups. Reduction of the 7-nitro group in compound **11** with iron powder and HCl made the 7-amino-2-morpholino-4-methoxyquinazoline (**12**) available (85% yield). Molecular structure and purity of the obtained quinazoline derivatives **2**, **4a-d**, **7a-g**, **8a-d**, **9a-d**, **10-12** were unequivocally confirmed by ^1H and ^{13}C NMR, elemental analysis, and HRMS data. All compounds are thermally stable with decomposition temperatures determined by thermogravimetric analysis (TGA) for compounds **8b**, **8c**, and **8d** to be 233, 212, and 204 °C, respectively.

10.1002/asia.202100534

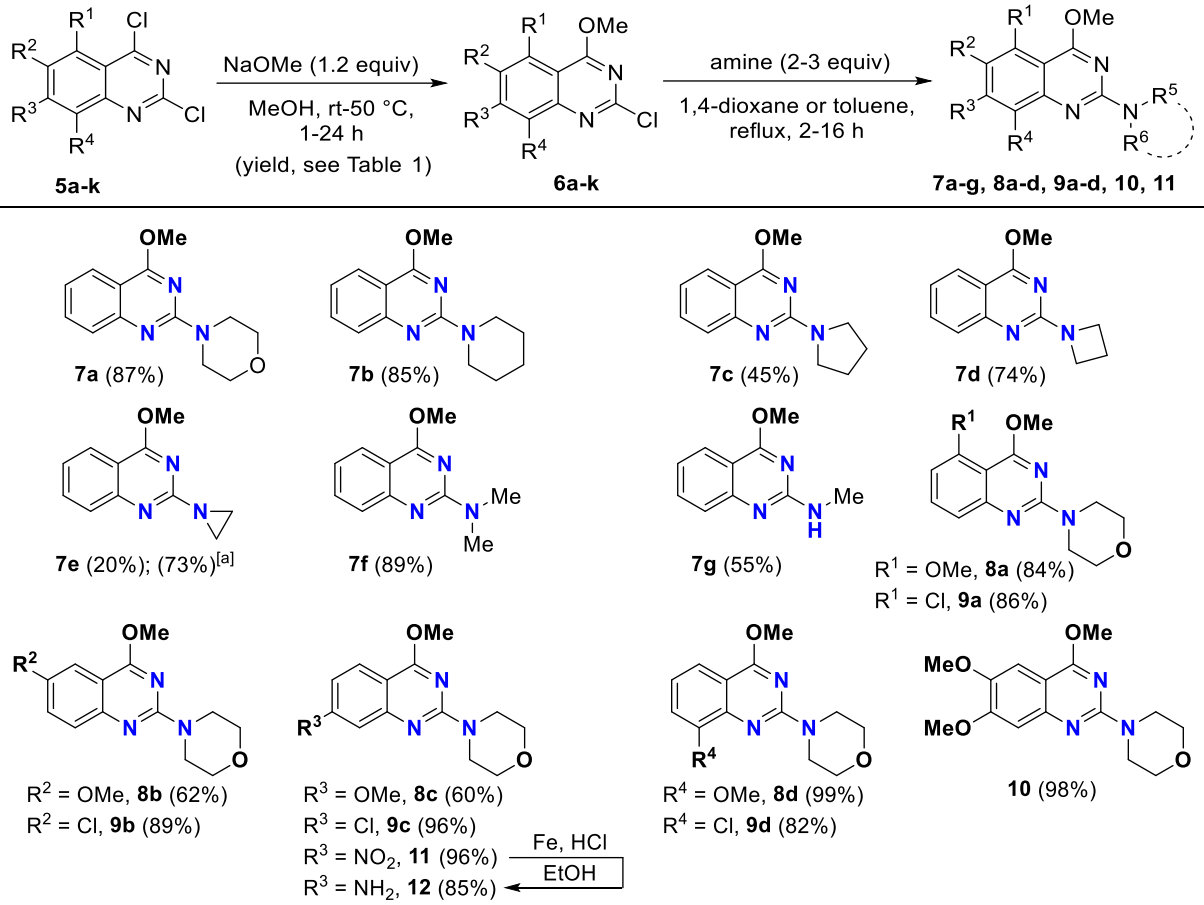

Scheme 2 Synthesis of 2-amino-4-methoxyquinazolines by side selective S_NAr reactions starting from substituted 2,4-dichloroquinazolines **5a-k**. Yield of **6a-k**, see Table 1; yield of isolated compounds **7a-g**, **8a-d**, **9a-d**, and **10-12** after column chromatography in parenthesis. [a] 3 mol% $Pd(OAc)_2$, 4 mol% Xantphos (4,5-bis(diphenylphosphino)-9,9-dimethylxanthene**)**, Cs_2CO_3, toluene, aziridine, 3 d at 100 °C in a sealed Schlenk tube.

Table 1. Reaction of 2,4-dichloroquinazolines **5** with sodium methanolate to give 2-chloro-4-methoxyquinazolines **6**.

5	R^1	R^2	R^3	R^4	6	Yield, %[a]
5a	H	H	H	H	**6a**	60
5b	OMe	H	H	H	**6b**	74
5c	Cl	H	H	H	**6c**	49
5d	H	OMe	H	H	**6d**	59
5e	H	Cl	H	H	**6e**	67
5f	H	H	OMe	H	**6f**	91
5g	H	H	Cl	H	**6g**	82
5h	H	H	H	OMe	**6h**	56
5i	H	H	H	Cl	**6i**	57
5j	H	OMe	OMe	H	**6j**	87
5k	H	H	NO_2	H	**6k**	66

[a] Yield based on isolated material after column chromatography on silica gel.

The x-ray crystal structures of compounds **8d**, **10**, and **11** are displayed in Figure 2. Notably, all three solid state molecular structures show the *N*-morpholino substituent at the quinazoline 2-position in a conformation allowing efficient conjugation of the morpholino nitrogen lone pair with the electron deficient heteroaromatic core – as one would expect for a rational electronic push-

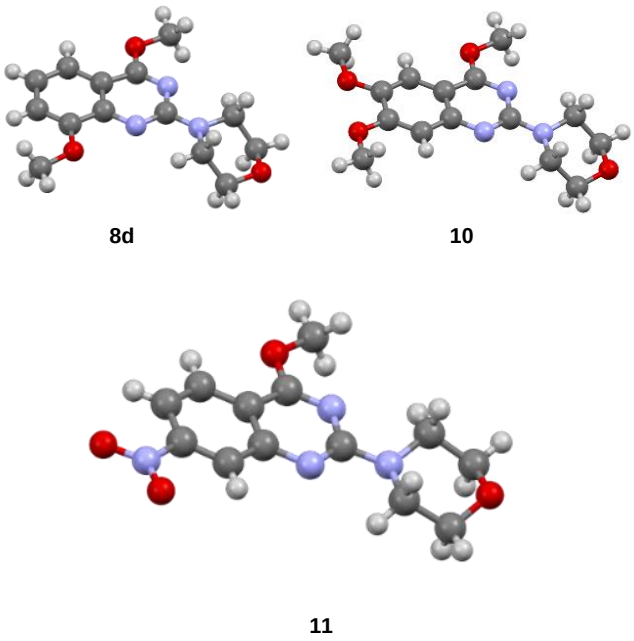

Figure 2. Molecular structure of quinazolines **8d (**CCDC: 2081760), **10 (**CCDC: 2081761), and **11 (**CCDC: 2081759) in the single crystal.

10.1002/asia.202100534

pull system. Here, the *N*-morpholino group is acting as the electron donor and the electron deficient heteroaromatic core as the acceptor. The extent of conjugation is also displayed by an essentially trigonal planar morpholino *N*-atom, as given by the sum of the angles around the nitrogen atom ($\Sigma N\alpha$) which is 359°, 357°, and 351° for **8d**, **10**, and **11** respectively. The crystal packing of quinazolines **8d** and **10** show no significant intermolecular contacts and that is one reason why PLE properties of solution and solids are very similar (see next paragraph on photophysical properties). In contrast, the packing of quinazoline **11** in the single crystal shows a "π-stacked" molecular arrangement with a 339 pm distance between two heteroaromatic units (for details, see supporting information). Its solid state PLE differs significantly from the one in solution.

Photophysical properties in solution and solid state

The quinazolines **2**, **4a-d**, **7a-g**, **8a-d**, **9a-d**, and **10-12** were examined by UV-vis absorption and steady-state fluorescence spectroscopy in solution and solid state together with their respective quantum yields. Relevant photophysical data are compiled in Table 2. Solution spectra were taken in concentrations of 10^{-5} *M* in order to avoid intermolecular interaction or aggregation of the solutes. Quantum yields were determined with an absolute photoluminescence quantum yield measurement system (Hamamatsu C9920-02).[37] All samples were deoxygenated by purging the respective solution with argon for 20 minutes prior to measurement. Examples of UV-vis and photoluminescence emission (PLE) spectra of the quinazolines **2** and **4a-d** are displayed in Figure 3 (for the complete set of UV-vis & PLE spectra, see supporting information).

With a low-energy band at $^{abs}\lambda_{max}$ (CH_2Cl_2) = 326 nm and a molar absorption coefficient of ε = 6700 L mol^{-1} cm^{-1} the UV-vis absorption spectra of 4-*N*-morpholinoquinazoline **2** significantly distinguishes from its regioisomer **4a** with a characteristic broad red-shifted absorption at $^{abs}\lambda_{max}$ (CH_2Cl_2) = 372 nm (ε = 2900 L mol^{-1} cm^{-1}). Such a characteristic low-energy absorption band with its underlying n-π* intramolecular charge transfer (ICT) is also found for other 2-*N*-morpholino quinazolines; i.e. **4b-d** with respectively $^{abs}\lambda_{max}$ (CH_2Cl_2) = 372, 366, 384, and 362 nm.

Notably, quinazoline **2** with a 4-*N*-morpholino group is non fluorescent in solution and solid state, whereas the quinazolines **4a-d** having a 2-*N*-morpholino group reveal a bright fluorescence with PLE intensity maxima ranging from $^{em}\lambda_{max}$ (CH_2Cl_2) = 426-446 nm and with quantum yields of ϕ_F = 0.39-0.65 (Table 2). This clearly indicates that the *N*-amino group in 2-position of the quinazoline scaffold is essential for an intense light emission and acts as a fluorescence "turn-on unit" with respect to fluorescence-structure-property relationships (FSPR). Likewise, the substituent in 4-position alters the light emission wavelength with $^{em}\lambda_{max}$ (CH_2Cl_2) = 446, 440, and 478 nm, for a *N*-morpholino-, methyl-, or phenyl group respectively (Table 2).

Further insight into the FSPR of 2-*N*-aminoquinazolines was obtained with the 2-*N*-amino-4-methoxyquinazolines **7a-g** having *N*-amino substituents of varying ring size and electron donor strength. Their UV-vis absorption spectra all display the characteristic broad ICT band in the 300-400 nm region and the

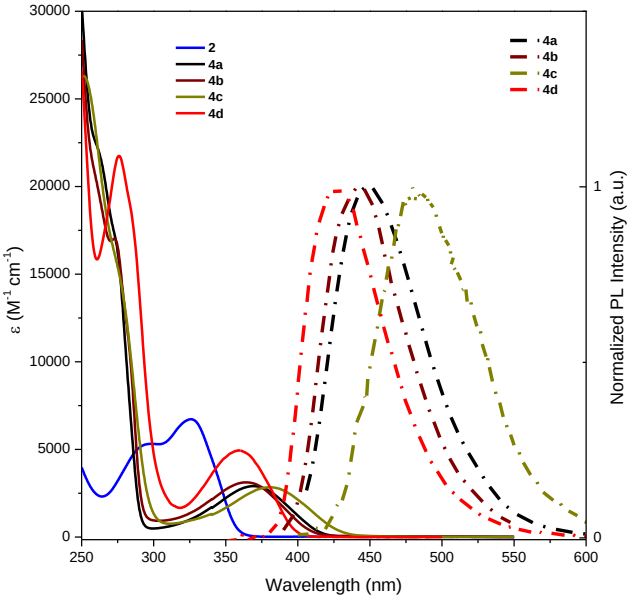

Figure 3. UV-vis absorption (solid lines) and photoluminescence emission (dotted lines) of the quinazolines **4a-d** (c = 10^{-5} M). 4-(*N*-morpholino)quinazoline **2** is non-emissive in solution.

absorption maxima $^{abs}\lambda_{max}$ tend to be red-shifted – as does the corresponding $^{em}\lambda_{max}$ in the PLE spectra – with an increase of the donor strength of the 2-*N*-amino substituent (Figure 4). This bathochromic shift of the ICT absorption band follows the order **7e** (*N*-aziridine), **7g** (-NHMe), and **7f** (-NMe_2) with $^{abs}\lambda_{max}$ (CH_2Cl_2) = 318, 353, and 339 nm respectively. The same trend is observed for the PLE spectra with $^{em}\lambda_{max}$ (CH_2Cl_2) = 376, 392, and 411 nm for respectively **7e**, **7g**, and **7f** having Stokes shifts of 3990-4850 cm^{-1}. The *N*-morpholino moiety at position 2 of the quinazoline scaffold is a considerable weaker electron donor than the respectively *N*-piperidine unit as the former has an electronegative oxygen in the heterocyclic 6-membered ring - compared to a –CH_2- unit of the latter. Although this effect is small it can be seen by a slight hypsochromic shift of both the maxima of the ICT absorption (8 nm) as well as the PLE emission band (4 nm) of the *N*-morpholinoquinazoline **7a** compared to the *N*-piperidino derivative **7b** in CH_2Cl_2 (Table 2). The influence of the electron donor strength of the 2-*N*-amino substituent on the photoluminescence properties is furthermore visualized by a correlation attempt of the Hammett substitution parameter σ_p of different amine substituents with the PLE maxima of the quinazolines **7a-g** (Figure 4, insert).[38, 39]

Notably, the solution quantum yields within this set of 2-*N*-aminoquinazolines also differ significantly with the amino donor capacity. For instance, the quinazolines **7e** (*N*-aziridine) and **7g** (-*N*MeH) have solution quantum yields of ϕ_F (CH_2Cl_2) = 0.38 and 0.49 respectively; whereas the quinazolines **7a-d**, and **7f** have much higher solution PLE quantum yields of ϕ_F (CH_2Cl_2) = 0.61-0.68. In the quinazoline-(**7a-g**)-series, the highest quantum yield in solution was found for the 2-*N*-azetidino-4-methoxyquinazoline

10.1002/asia.202100534

Table 2. Spectroscopic properties of quinazolines **2**, **4a-d**, **7a-g**, **8a-g**, **9a-d**, and **10-12** in solution and solid state.

Solution (10^{-5} *M* in CH_2Cl_2)						Solid (crystals)	
Compd.[a]	UV-vis $^{abs}\lambda_{max}$, nm, (ε, M^{-1} cm^{-1})	UV-vis $^{abs}\lambda_{onset}$, nm	PLE^{solution} $^{em}\lambda_{max}$, nm	ϕ_F[b], solution (λ_{ex}, nm)	Stokes shift cm^{-1}	PLE^{solid} $^{em}\lambda_{max}$, nm	ϕ_F, solid (λ_{ex}, nm)
2	326 (6700)	358	-[c]	-[c]	-[c]	-[c]	-[c]
4a	372 (3000)	419	446	0.39 (330)	4460	449	0.23 (330)
4b	366 (3300)	412	440	0.42 (340)	4600	-[c]	-[c]
4c	384 (3900)	433	478	0.43 (380)	5120	475	0.03 (380)
4d	362 (5200)	401	426	0.65 (340)	4150	434	0.55 (330)
7a	347 (3000)	386	411	0.62 (340)	4550	423	0.16 (330)
7b	355 (3100)	393	415	0.61 (330)	4010	417	0.37 (330)
7c	354 (3500)	391	415	0.64 (330)	4150	413	0.35 (330)
7d	346 (3600)	385	410	0.68 (330)	4510	426	0.54 (330)
7e	318 (3400)	346	376	0.38 (310)	4850	400	0.12 (310)
7f	353 (3400)	388	411	0.61 (330)	4000	415	0.49 (320)
7g	339 (3300)	372	397	0.49 (330)	3990	418	0.04 (320)
8a	345 (3000)	380	405	0.50 (330)	4300	412	0.15 (360)
8b	365 (3600)	404	430	0.73 (330)	4140	435	0.41 (340)
8c	332 (4900)	366	395	0.43 (330)	4800	389	0.30 (320)
8d	350 (3100)	386	412	0.67 (330)	4300	417	0.37 (340)
9a	354 (3200)	393	416	0.35 (330)	4210	437	0.05 (330)
9b	361 (3100)	400	425	0.47 (330)	4170	425	0.12 (330)
9c	350 (2900)	389	415	0.28 (330)	4480	425	0.21 (330)
9d	358 (3700)	395	420	0.54 (330)	4120	455	0.03 (330)
10	345 (6200)	380	404	0.65 (345)	4230	407	0.37 (340)
11	412 (1700)	480	-[c]	-[c]	-	552	0.07 (400)
12	335 (6800)	366	395	0.13 (330)	4540	-[c]	-[c]

[a]Spectra were recorded at room temperature at $c = 10^{-5}$ *M* in dichloromethane. [b]Determined with an integration sphere after purging the solution with argon for 20 min.[37] [c]Compound is non fluorescent.

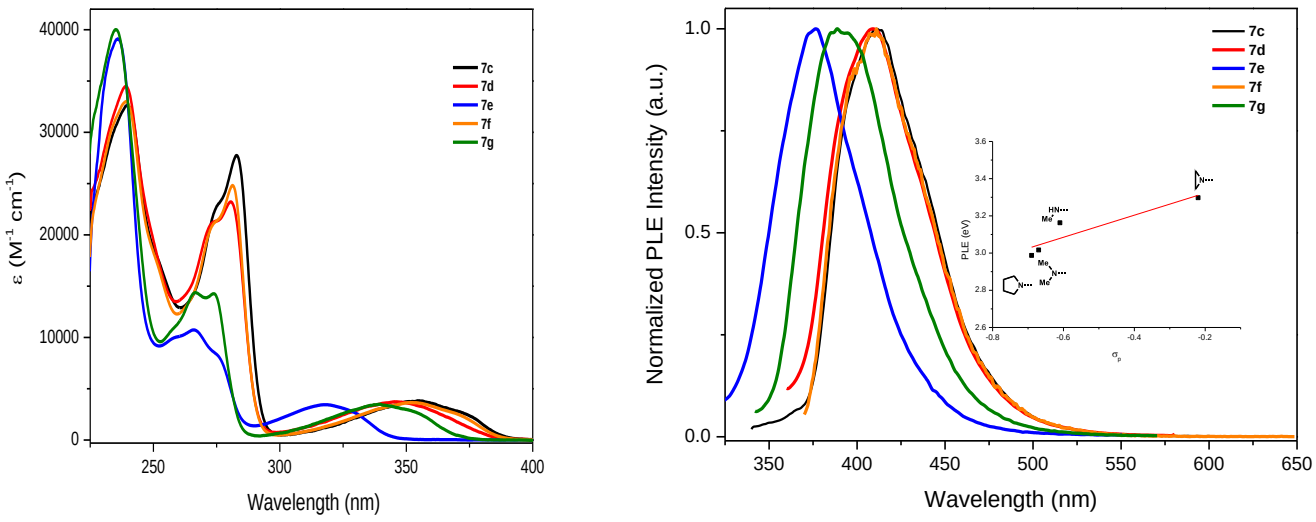

Figure 4. Comparative absorption (left) and photoluminescence emission spectra (right) of representative 2-*N*-amino -4-methoxyquinazolines with varying *N*-amino substituents recorded in CH_2Cl_2 (c = 10^{-5} M). Insert: Correlation of the Hammett substitution parameter σ_p with the PLE intensity maxima (eV).

10.1002/asia.202100534

(**7d**) with ϕ_F (CH_2Cl_2) = 0.68. Such an increase in fluorescence efficiency is most likely due to a comparable higher rigidity of the 4-membered ring paired with its still present strong electron donor capacity. Evidently, the increase in electron donor strength of the 2-*N*-amino substituents is along with an increase of the ICT performance of the excited state following the n-π* transition to the ^{1}CT* state and therefore, effecting an increase in the photoluminescence efficiency. This trend is preserved by quantum yields determined from the solid state (Table 2).

The UV-vis absorption and PLE emission characteristics of methoxy-(**8a-d**) and chloro-(**9a-d**) substituted 2-*N*-morpholino-4-methoxyquinazoline having a substituent in either 5-, 6-, 7-, or 8-position were also evaluated (Table 2). Both sets show alternating influences in affecting absorption and PLE wavelengths by shifting the substituent from the 5- to the 6-, to the 7-, and finally to the 8-position. Within each set the largest red-shift in PLE is observed with a substituent at the 6-position of the quinazoline core - i.e. for **8b** and **9b** with $^{em}\lambda_{max}$ = 430 and 425 nm, respectively. This trend is conserved by quantum yield measurements in solution, that give with ϕ_F = 0.73 and 0.47 for respective **8b** and **9b** the highest values in each series.

Fluorescence spectra of quinazoline **7b** were recorded in solvents of different polarity and the respective Stokes shifts were correlated with Reichardt's normalized solvent polarity parameter E_T^N (Figure 5).[40] The observed positive solvatochromism displays the stabilization of a highly polarized excited charge transfer state (^{1}CT*) by a more polar solvent. It clearly confirms a considerable intramolecular charge transfer (ICT) on excitation from a less dipolar ground state to a highly dipolar excited state molecule. Such a positive solvatochromism is also found with all other investigated 2-*N*-aminoquinazolines (see supporting information).

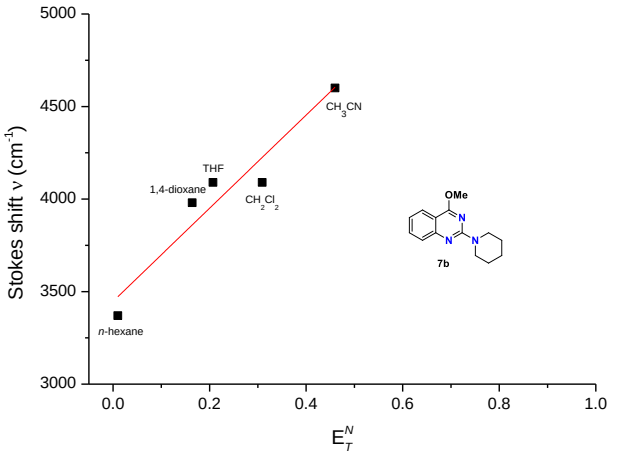

Figure 5. Solvatochromism of 2-*N*-piperidino-4-methoxyquinazoline (**7b**). Correlation of Reichardt's normalized polarity parameter E_T^N with obtained Stokes shift. E_T^N values: 0.009 (*n*-hexane), 0.164 (1,4-dioxane), 0.207 (THF), 0.309 (CH_2Cl_2), and 0.460 (CH_3CN).

Although photoluminescence emission from solids is often quenched by molecular aggregates, most of the 2-*N*-amino-4-methoxyquinazolines show a bright fluorescence from the solid state with considerable high quantum yields (Table 2). The solid state PLE spectra are very similar to the ones obtained from solution with respect to emission maxima and band shape indicating that the respective molecular conformation in solution and solid state must be quite similar. Consequently, intermolecular interactions affecting fluorescence emission are very weak or absent in the solid state (Figure 6, for the complete set of solid state PLE spectra, see supporting information).

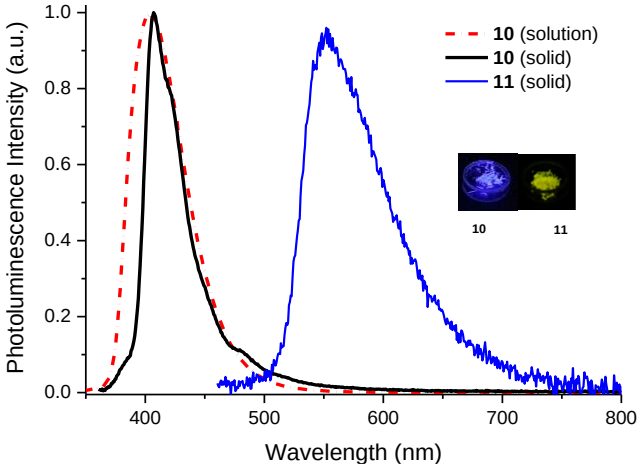

Figure 6. PLE spectra of 2-*N*-morpholino-4,6,7-trimethoxyquinazoline (**10**) in solution and from solid state; and solid state PLE spectra of 2-*N*-morpholino-7-nitro-4-methoxyquinazoline (**11**). Compound **11** is non-fluorescent in solution. Insert: Quinazolines **10** and **11** (solid) under UV-lamp.

A notable exception is the 7-nitro-quinazoline **11** that is non-fluorescent in solution but displays a yellow solid state fluorescence with $^{em}\lambda_{max}$ = 552 nm. This remarkable red-shifted fluorescence that distinguishes **11** from all other investigated 2-*N*-morpholinoquinazolines is most likely originated from "π-stacked"-type aggregates in the crystal and points to excimer-type light emission.[41] However, the possibility of room temperature phosphorescence due to a "locked conformation" in the crystal lattice cannot be ruled out at this point.

Electrochemical properties & HOMO/LUMO energy levels

Electrochemical properties of the quinazolines **2**, **4a-d**, **7a-g**, **8a-d**, and **9a-d** were investigated by cyclic voltammetry and the results are summarized in Table 3. Cyclic voltammetry experiments were carried out at a scan rate of 100 mV/s with a three-electrode set-up under an argon atmosphere and with a Pt electrode as the working and calomel (SCE) as the reference electrode. *n*Bu_4NPF_6 (0.1 *M* in CH_2Cl_2) was used as the electrolyte solution and Fc/Fc^+ (ferrocene / ferrocenium redox couple: 0.46 V vs SCE) as the internal standard for calibration purpose. Representative cyclic voltagram curves of the quinazolines **2**, **4a**, **7a**, and **8b** with respect to their oxidation potential are displayed in Figure 7.

Reduction potentials could not be measured as the electrochemical window in CH_2Cl_2 used ranged from -1.9 to 1.9 V (for the full set of cyclic voltagrams, see supporting information). Within the solvent/electrolyte electrochemical window the 2-*N*-morpholinoquinazoline **2**, the 4-*N*-morpholinoquinazoline **4a** and the 2-*N*-morpholino-4-methoxyquinazoline **7a** display an irreversible first oxidation potential of $^{ox}E_{1/2}$ = 1.60, 1.32 and 1.18 eV respectively (Figure 7 and Table 3). Notably, the first oxidation product of the 4,6-dimethoxy-2-*N*-morpholinoquinazoline (**8b**) is more stable under the reaction conditions and displays a quasi-reversible first oxidation potential with $^{ox}E_{1/2}$ = 1.09 V.

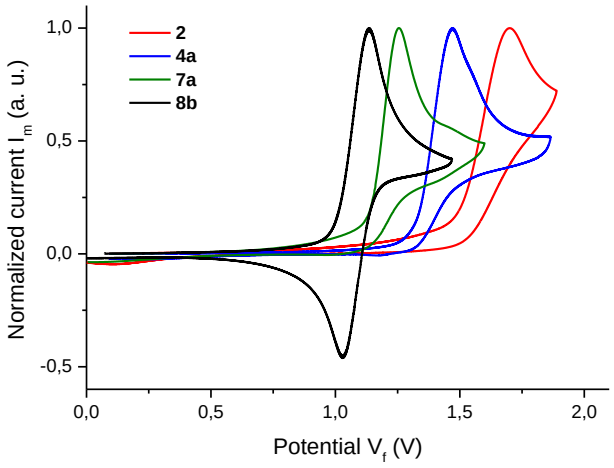

Figure 7. Cyclic voltammetry of 2-*N*-morpholinoquinazoline (**2**), 4-*N*-morpholinoquinazoline (**4a**), 2-*N*-morpholino-4-methoxyquinazoline (**7a**), and 4,6-dimethoxy-2-*N*-morpholinoquinazoline (**8b**). Each sample was recorded in deoxygentated solutions with $c = 10^{-3}$ *M* in CH_2Cl_2/0.1 *M* nBu_4NPF_6 at room temperature. Scan rate 100 mV/s, working electrode Pt, auxiliary electrode Pt wire, and SCE as the reference electrode. The potentials were corrected against Fc/Fc^+ as internal reference.

The decrease of oxidation potentials in this set of quinazolines **2**, **4a**, **7a** and **8b** clearly reveals the influence of the *N*-amino substituent and its position by lowering the oxidation potential significantly when placed from the 4-position (quinazoline **2**) to the 2-position (quinazoline **4a**).
Furthermore, the influence of the two methoxy groups acting as electron donor in compound **8b**, that additionally lower the oxidation potential, is also disclosed by these measurements.

From the onset of the first oxidation half-wave ($^{ox}E_{onset}$) the HOMO energy level for the quinazolines **2**, **4a-d**, **7a-g**, **8a-d**, and **9a-d** were estimated with: $E_{HOMO} = -(^{ox}E_{onset,\ vs\ Fc/Fc+} + 5.10)$ (eV) for measurements in dichloromethane solution with 0.1 *M* nBu_4NPF_6 as the supporting electrolyte.[42] The half-wave potential for the Fc/Fc^+ redox-couple was set to $E_{1/2} = 0.46$ eV for calibration purpose.[43] We chose -5.10 eV as the formal potential of the Fc/Fc^+ redox couple in the Fermi scale.[44] The HOMO energy level for the 4-*N*-morpholino-2-methoxyquinazoline **7a** was thus estimated to $E_{HOMO} = -5.78$ eV. The energy level of the lowest unoccupied molecular orbital (LUMO) was calculated by adding the value of the optical band gap ($^{opt}E_g$) taken from the onset of the long-wavelength absorption band of the UV-vis absorption spectra in CH_2Cl_2 to the HOMO energy level with $E_{LUMO} = E_{HOMO} + {}^{opt}E_g$. For quinazoline **7a** the LUMO energy was therefore found to be $E_{LUMO} = -2.54$ eV. The experimentally established HOMO/LUMO energy levels, together with the values for the optical band gap of all synthesized and investigated *N*-aminoquinazolines are listed in Table 3.

A comparison of photoluminescence emission data (Table 2) with empirical HOMO/LUMO energy values (Table 3) and with the corresponding band gap energies ($^{opt}E_g$) reveals that 2-*N*-aminoqunazolines with high HOMO energy levels and small band gap values display the highest fluorescence quantum yields. Concerning FSPR this points to that the fluorescence properties of 2-*N*-aminoquinazolines are basically attributed to the extent of ICT and polar charge transfer in the excited state. The latter is influenced by a strong electron donor (*N*-amino group) in 2-position and is enforced/quenched by peripheral donor substituents on the 4-, as well as the 5-, 6-, 7, or 8-positions. For instance, in the comparable series of 2-*N*-amino-4-methoxyquinazolines **7a-g**, **8a-d**, and **9a-b**, the 2-*N*-morpholino-4,6-dimethoxy-quianzoline (**8b**) displays the highest fluorescence quantum yield ($\phi_F = 0.73$), together with the highest HOMO energy level ($E_{HOMO} = -5.60$ eV) and the lowest optical band gap ($^{opt}E_g = 3.03$ eV).

Table 3. Experimental Data for HOMO, LUMO, and Band Gap Energies and Calculated Data for HOMO, LUMO, and Excited State Energies.

Compd.	Experimental data					Calculated data[a]		
	$^{ox}E_{1/2}$ (V)	$^{ox}E_{onset}$ (eV)	$^{opt}E_g$ (eV)	E_{HOMO} (eV)	E_{LUMO} (eV)	$^{calc}E_g$ (eV)	$^{calc}E_{HOMO}$ (eV)	$^{calc}E_{LUMO}$ (eV)
2	1.60	1.52	3.47	-6.16	-2.69	3.89	-6.32	-1.89
4a	1.32	1.31	2.97	-5.95	-2.99	3.37	-5.91	-2.04
4b	1.33	1.24	3.01	-5.88	-2.87	3.41	-5.85	-1.82
4c	1.38	1.27	2.86	-5.91	-3.05	3.24	-5.88	-2.07
4d	1.13	1.07	3.09	-5.71	-2.62	3.48	-5.73	-1.66
7a	1.18	1.14	3.24	-5.78	-2.54	3.62	-5.82	-1.58
7b	1.17	1.04	3.17	-5.68	-2.51	3.53	-5.68	-1.53
7c	1.19	1.03	3.17	-5.67	-2.50	3.53	-5.65	-1.51
7d	1.27	1.13	3.22	-5.77	-2.55	3.60	-5.78	-1.56
7e	--	1.48	3.57	-6.12	-2.55	3.96	-6.26	-1.71
7f	1.24	1.10	3.17	-5.74	-2.57	3.58	-5.73	-1.54
7g	1.35	1.20	3.29	-5.84	-2.55	3.63	-5.82	-1.59
8a	1.13	1.09	3.27	-5.73	-2.46	3.69	-5.72	-1.40
8b	1.09	0.96	3.03	-5.60	-2.57	3.34	-5.52	-1.64
8c	1.22	1.16	3.39	-5.80	-2.41	3.72	-5.81	-1.47
8d	1.14	1.04	3.19	-5.68	-2.49	3.58	-5.60	-1.43
9a	1.35	1.26	3.15	-5.90	-2.75	3.53	-5.91	-1.76
9b	1.38	1.22	3.10	-5.86	-2.76	3.46	-5.86	-1.80
9c	1.35	1.30	3.19	-5.94	-2.75	3.57	-5.95	-1.75
9d	1.36	1.28	3.14	-5.92	-2.78	3.51	-5.90	-1.77

[a] calculated with DFT using TDDFT/BLYP3 functional in CH_2Cl_2 (PCM).

Theoretical calculations

Ab initio molecular orbital (MO) and configuration interaction (CI) calculations on the synthesized quinazolines were carried out with the aim to gain further insight into HOMO-LUMO energy levels, the first electronically excited state (S_1) energies, and their electronic structures, and to compare the value of experimental data with *ab initio* result.

Polarizable continuum model (PCM)[45] was assumed to take account of solvation effect with dichloromethane at each *ab initio* calculation. Møller–Plesset second-order perturbation theory (MP2) and density functional theory (DFT) with B3LYP[46] and M062X[47] functionals were first employed to optimize molecular geometries for the electronic ground state (S_0, X^1A). The vertical excitation-energies to five lower-lying electronic

10.1002/asia.202100534

excited states ($2^1A(S_1)$, 3^1A, 4^1A, 5^1A and 6^1A in C_1 symmetry) were then determined by a single-point calculation for the symmetry-adapted cluster/configuration interaction (SAC-CI)[48] calculations at the MP2-optimized geometry, while time-dependent DFT (TDDFT)[49] calculation was used at B3LYP and M062X functionals with DFT-optimized geometry. All the *ab initio* computations were performed using Gaussian 16 program package[50] with the aug-cc-pVDZ basis set.[51-52]

The orbital energy-values for the calculated HOMO and LUMO levels with DFT TDDFT/B3LYP are listed in Table 3 (for other levels of calculation, see supporting information). These energy-levels are linearly correlated with experimentally determined band gaps. Figure 8 displays the comparison of empirically determined HOMO/LUMO energy levels via a combination of electrochemical and optical measurements, and calculated ones obtained from DFT methods using the TDFFT/BLYP3 functions. Figure 9 shows the correlation between experimentally estimated optical band gaps ($^{opt}E_g$) and the calculated first excitation energies ($^{calc}E_g$), as well as the correlation between empirical HOMO energies obtained by electrochemical methods and the calculated HOMO energy levels.

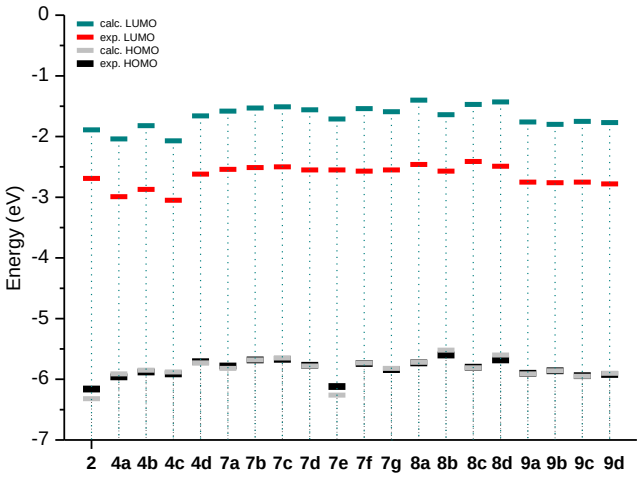

Figure 8. Compilation of empirical and theoretical obtained HOMO-LUMO energy levels. Calculation level DFT TDDFT/B3LYP in CH_2Cl_2.

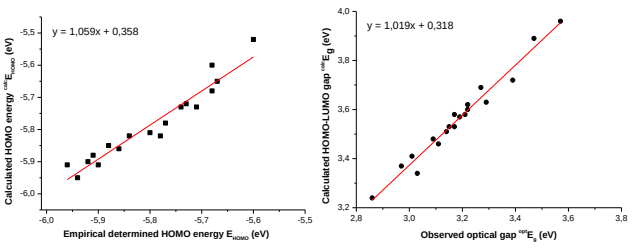

Figure 9. (left) Correlation between HOMO energy levels obtained by electrochemical methods (E_{HOMO}) and calculated HOMO energies ($^{calc}E_{HOMO}$). (right). Correlation of observed and calculated gaps: $^{opt}E_g$ vs $^{calc}E_g$. Calculation level DFT TDDFT/B3LYP in CH_2Cl_2 (PCM) for both.

We observe a reasonable good linear correlation between the experimentally obtained HOMO energy by electrochemical means and the respective calculated ones by DFT TDDFT/BLYP in CH_2Cl_2 (PCM) (Figure 9, left). And although the optical gap ($^{opt}E_g$) - that is assumed to correspond to the energy of the lowest electronic transition via absorption of a single photon is affected by the strong binding energy between hole and electrons (exciton binding energy) - *per se* differs (is lower in energy) from the calculated HOMO-LUMO gap ($^{calc}E_g$) – that provides an approximation of the fundamental gap[53-54] - we found a fair trend of $^{opt}E_g$ vs $^{calc}E_g$. Both follow the respective changes in the substitution pattern of the quinazoline luminophore and mirror the quality of the obtained data (Figure 8 and Figure 9). However, the orbital energy-differences between HOMOs and LUMOs are larger than the experimental data by ca. 0.5 eV. The results obtained by DFT/M062X showed large differences by ca. 3.0 eV (see supporting information). These errors can be attributed to ignoring Coulomb- and exchange-integrals. On the other hand, TDDFT/ B3LYP and TDDFT/M062X showed better values which are given by vertical electronic excitation energies for S_1 state. This result implies that the molecules are not aggregated. However, there is still an error of ca. 0.5 eV between TDDFT/B3LYP and experimental data (Table 3 and Figure 8). However, the data follow the overall experimentally observed trend in HOMO/LUMO energy changes with variations in the substitution pattern; i.e. the donor strength in position 2 of the quinazoline (Figure 8).

Table 4. Electron correlation interaction (CI) coefficients and electron configuration state functions (CSF) of the S_1 (2^1A in C_1 symmetry) state determined by SAC-CI calculation; digit with "a" in parenthesis shows molecular orbital (MO) in C_1 and "(57a) → (64a)" is a single-electron excitation from 57th MO to 64th. (MOs shown in Figure 10 and supporting information).

Compound	CI coefficient	CSF	Character of excitation
2	-0.79620	(57a) → (64a)	π–π*
	0.27858	(57a) → (65a)	π–Ryd
	0.21625	(56a) → (64a)	π–π*
4a	0.89667	(57a) → (64a)	π–π*
	0.14357	(56a) → (74a)	π–Ryd
7a	0.80843	(65a) → (75a)	π–π*
	0.36835	(65a) → (76a)	π–Ryd
7c	-0.71178	(61a) → (72a)	π–Ryd
	-0.44801	(61a) → (71a)	π–Ryd
	0.35266	(61a) → (73a)	π–Ryd
7d	-0.83333	(57a) → (66a)	π–Ryd
	0.27774	(57a) → (65a)	π–Ryd
7e	0.79086	(53a) → (61a)	π–π*
	-0.39161	(53a) → (60a)	π–Ryd
7f	-0.60684	(54a) → (63a)	π–Ryd
	0.54282	(54a) → (62a)	π–Ryd
	-0.37324	(54a) → (64a)	π–Ryd
7g	-0.88260	(50a) → (58a)	π–π*
	0.15897	(50a) → (57a)	π–Ryd

10.1002/asia.202100534

In order to confirm the effect of the electron-correlation energy, we also performed SAC-CI calculations (Table 4). SAC-CI theory could provide us the similar result to Full-CI approach. The electronic character of **2** was described by a single-electron excitation to Rydberg (Ryd) type of MO (65a) from HOMO, "(57a) → (65a)", with the main configuration of π-π* which is "(57a) → (64a)" excitation. The ICT property was theoretically described as the excitation to Rydberg-MO at Hartree-Fock (HF) level—SAC-CI theory is based on HF theory. If multi-configuration (MC) / multi-reference (MR) theory such as MCSCF and MR-CI were employed, the MOs would be different from Ryd-MOs described in SAC-CI, which can be interpreted as the MOs for n-π* excitation. The HF theory can, however, optimize only electronically occupied orbitals at variation principle. Virtual orbitals including Ryd-MOs are not optimized at self-consistent field (SCF) calculation. This problem could be resolved in multi-electron excitations (up to quartet-electron excitation) computed by SAC-CI method as it would be also done by Full-CI. As shown in Figure 10, there appear to be two groups in spectra for a series of **7c**–**7g**: One group

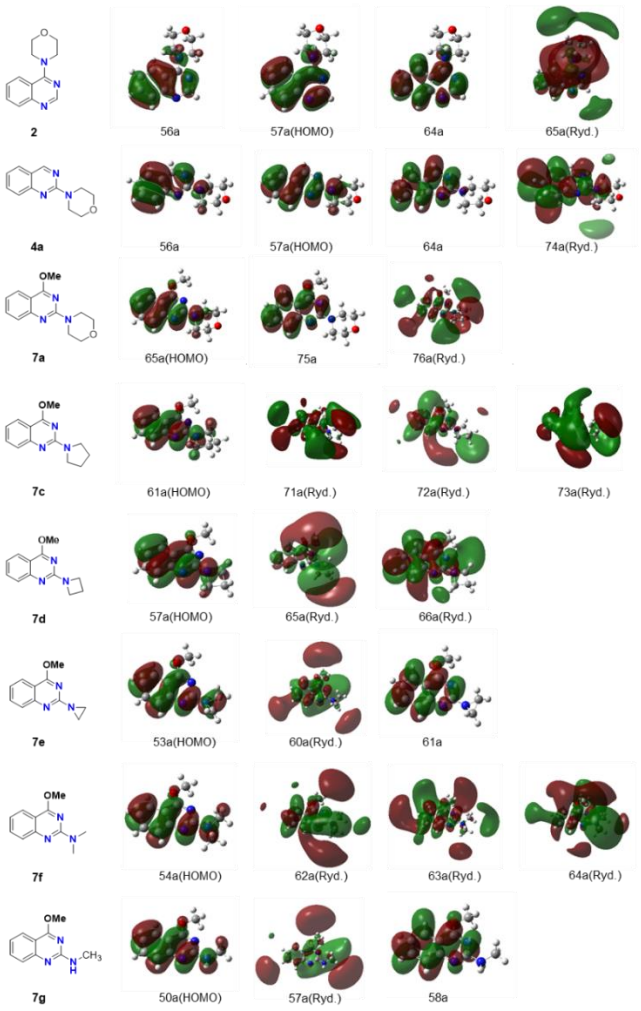

Figure 10. Molecular orbitals (MOs) to describe the S_1 state in SAC-CI calculations; digit with "a" in parenthesis shows molecular orbital (MO) in C_1 symmetry and "56a" is the 56th MO in C_1.

consists of **7e** and **7g**, and the other consists of **7c**, **7d** and **7f**. Since the primary electronic configurations of **7e** and **7g** are π-π* excitation with the minor contribution of π-Ryd (see Table 4), the ICT-character is weak and the S_1 state could not be stabilized in polar solution. On the other hand, the only ICT-characters (π-Ryd excitation) appear as the primary configurations for **7c**, **7d** and **7f**. S_1 could be strongly stabilized in polar solution, and thus the PLE would happen red-shifted - at the lower energy side - compared to **7e** and **7g**. A fact that is confirmed by empirical photophysical and fluorescence spectroscopy results in Figure 4.

Proton sensitive "turn-on" fluorescence molecular probe

UV-vis absorption and photoluminescence emission of 7-amino-2-*N*-morpholino-4-methoxyquinazoline **12** change both significantly under acidic conditions. Light absorption at the low-energy ICT band of **12** ($^{abs}\lambda_{max}$ = 335 nm) increases on subsequent addition of aliquots of trifluoro acetic acid (TFA) to a solution of quinazoline **12** in dichloromethane and the fluorescence emission intensity with band maxima at $^{em}\lambda_{max}$ = 395 nm increases in the same extent. This makes quinazoline **12** suitable as "turn-on" fluorescence molecular probe for ratiometric sensing of acidic environments (Figure 11).

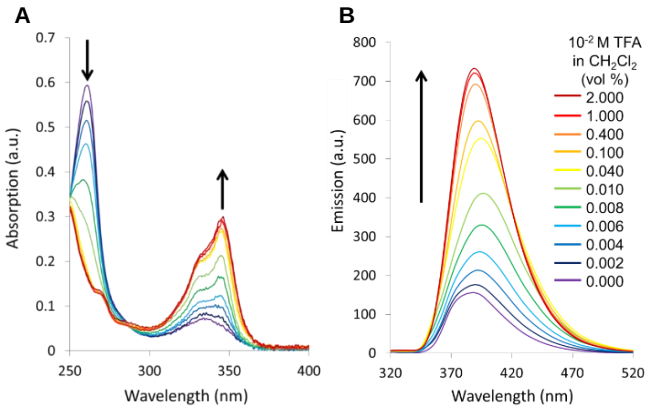

Figure 11. A) Successive changes of UV-vis absorption bands of 7-amino-2-morpholino-4-methoxyquinazoline (**12**) on addition of aliquots of trifluoro acetic acid (TFA). **B**) Fluorescence emission intensity enhancement of quinazoline **12** on ratiometric titration with TFA.

The fluorescence "turn-on" property of **12** is based on the 4.6-fold increase in fluorescence quantum yield, as verified with the help of an integration sphere. The solution quantum yield of "pure" non-protonated **12** was found to be ϕ_F (CH_2Cl_2, λ_{exc} = 330 nm) = 0.13 and increased to ϕ_F (CH_2Cl_2 + excess TFA, λ_{exc} = 330 nm) = 0.60 for the "protonated" **12**. The ratiometric titration of a 10^{-5} M solution of 7-aminoquinazoline **12** in CH_2Cl_2 at the excitation wavelength λ_{ex} = 293 nm (isobestic point in the UV-vis spectrum of **12**) by recording the fluorescence intensity at λ_F = 390 nm is shown in Figure 11-A. Saturation of the light emission intensity is reached with an approximate 10-fold excess of TFA. Notably, this increase in emission intensity upon protonation is reversible: Adding an excess of triethylamine (TEA) to a solution of **12** / TFA in CH_2Cl_2 results in a "turn-off" fluorescence and brings back the PLE spectra of the parent non-protonated **12** (Figure 11-B). An inter- or intramolecular photoinduced electron transfer (PET)[55] from the amino group at the 7-position towards the electron deficient quinazoline core of compound **12** is proposed to be the working principle of this molecular turn-on/off fluorescence probe. On protonation of the 7-amino group the PET is inhibited and

quinazoline **12** turns into a more efficient fluorophore comparable to those found with all other investigated derivatives of 2-*N*-amino-4-methoxy-quinazolines. However, other underlying mechanisms of fluorescence enhancement and quenching including reversible aggregate formation through hydrogen bonding cannot be ruled out yet and are objectives of future investigation.

Conclusion

We reported on the side-selective synthesis and full structure-photophysics characterization of a set of differently substituted *N*-amino-quinazolines as new small molecule fluorescence compounds. Aiming to disclose basic insights into fluorescence-structure-property relationship (FSPR) the synthesized quinazolines were evaluated by their photophysical and electrochemical properties. The amino group at position 2 of the quinazoline core proved to be essential for the fluorescence. The increase of electron donor strength of the 2-amino groups led to red-shifts in absorption and emission wavelengths and enhanced fluorescence efficiency in agreement with an effective ICT. Methoxy and chloro substituents at the position 6 caused larger bathochromic shifts than those at positions 5, 7, and 8. HOMO-LUMO energy levels were estimated by a combination of electrochemical and photophysical methods. Reasonable good linear correlations between empirical and theoretical HOMO/LUMO energies on the DFT TDDFT/BLYP in CH_2Cl_2 (PCM) were found. Furthermore, computation studies revealed that the excitation to the Rydberg-MOs in SAC-CI contributed to the ICT. The weakly fluorescent 7-amino derivative showed a significant increase in fluorescence emission intensity under acidic conditions and its quenching by the subsequent addition of a base revealed fluorescence "turn-on/off" properties. We believe that those 2-*N*-aminoquinazolines can function as fluorescent probes that sensitively respond to the environment, and can be utilized in molecular recognition as fluorophores.

Experimental Section

General procedure for the synthesis of 4-methoxy-2-chloro-quinazolines

2-Chloro-4,5-dimethoxyquinazoline (6b): A mixture of 2,4-dichloro-5-methoxyquinazoline[10, 56] (**5a**) (49.0 mg, 0.21 mmol) and sodium methoxide (17.4 mg, 0.32 mmol) was stirred in dry MeOH (10 mL) at 50 °C for 2 h. Column chromatography (SiO_2, hexane/ethyl acetate = 9:1 (v/v)) afforded compound **6b** (34.9 mg, 74% yield) as colorless solid, mp 112-113 °C; R_f = 0.18 (SiO_2, EtOAc/*n*-hexane = 1/9 (v/v)). ^{1}H NMR (300 MHz, $CDCl_3$): δ 3.98 (s, 3H), 4.18 (s, 3H), 6.90 (d, *J* = 4.8 Hz, 1H), 7.42 (d, *J* = 5.2 Hz, 1H), 7.71 (dd, *J* = 4.8, *J* = 5.2 Hz, 1H); ^{13}C NMR (125 MHz, $CDCl_3$): δ 55.4, 56.3, 106.6, 107.2, 119.1, 134.7, 154.4, 156.1, 157.4, 168.7. HRMS (EI) m/z calcd for $C_{10}H_9ClN_2O_2$ (M^+): 224.0353, found: 224.0350.

General procedure for the synthesis of 2-amino-4-methoxyquinazolines via S_NAr reaction.

2-*N*-Morpholino-4-methoxyquinazoline (7a): A mixture of 2-chloro-4-methoxyquinazoline (**6a**) (110 mg, 0.57 mmol) and morpholine (0.1 mL, 1.10 mmol) was stirred in 1,4-dioxane (5 mL) while heating to reflux for 5 h. Column chromatography (SiO_2, hexane/ethyl acetate = 4:1(v/v)) afforded compound **7a** (121 mg, 87% yield) as colorless solid; mp 90-91 °C; R_f = 0.24 (SiO_2, hexane/ethyl acetate = 1:4 (v/v)). ^{1}H NMR (300 MHz, $CDCl_3$): δ 3.80 (t, *J* = 4.8 Hz, 4H,), 3.91 (t, *J* = 4.8 Hz, 4H), 4.08 (s, 3H), 7.12-7.17 (m, 1H), 7.48-7.62 (m, 2H), 7.90-7.93 (m, 1H); ^{13}C NMR (125 MHz, $CDCl_3$): δ 44.6, 53.7, 67.0, 111.7, 122.0, 123.6, 125.0, 133.5, 153.2, 158.4, 167.4; HRMS (EI) m/z calcd for $C_{13}H_{15}N_3O_2$ (M^+): 245.1164, found: 245.1169.

2-*N*-piperidino-4-methoxyquinazoline (7b): To a solution of 2-chloro-4-methoxyquinazoline (**6a**) (200 mg, 1.03 mmol) in dry toluene (15 mL) was added piperidine (1.0 mL, 10.30 mmol). The reaction mixture was stirred at 110 °C overnight. Column chromatography (SiO_2, ethyl acetate/*n*-pentane = 1:20 (v/v)) afforded compound **7b** (213 mg, 85% yield) as solid, mp 58-60 °C; R_f = 0.47 (SiO_2, ethyl acetate/*n*-pentane = 1:20 (v/v)). ^{1}H NMR (400 MHz, $CDCl_3$): δ 1.73 – 1.59 (m, 6H), 3.90 - 3.88 (m, 4H), 4.08 (s, 3H), 7.09 (ddd, *J* = 7.9 Hz, *J* = 7.1 Hz, *J* = 0.8 Hz, 1H), 7.47 (d, *J* = 8.4 Hz, 1H), 7.56 (ddd, *J* = 8.3 Hz, *J* = 7.0 Hz, *J* = 1.3 Hz, 1H), 7.88 (d, *J* = 8.0 Hz, 1H); ^{13}C NMR (100 MHz, $CDCl_3$): δ 25.1, 26.1, 45.2, 53.7, 111.4, 121.4, 123.7, 124.9, 133.4, 153.8, 158.7, 167.3. HRMS (ESI) m/z calcd for $C_{14}H_{18}N_3O$ $(M+H)^+$: 244.1450, found: 244.1454.

2-*N*-Pyrrolidino-4-methoxyquinazoline (7c): Pyrrolidine (0.266 mL, 3.07 mmol) was added to a solution of 2-chloro-4-methoxyquinazoline (**6a**) (300 mg, 1.54 mmol) in 1,4-dioxane (20 ml), and the mixture was heated to refluxed for 2 h. Column chromatography (SiO_2, hexane/ethyl acetate = 4:1 (v/v)) gave **7c** (159 mg, 45% yield) as colorless solid, mp 93-94 °C; R_f = 0.30 (SiO_2, hexane/ethyl acetate = 4:1 (v/v)). ^{1}H NMR (500 MHz, $CDCl_3$): δ 7.89 (d, *J* = 8.1 Hz, 1H), 7.58-7.56 (m, 2H), 7.09 (m, 1H), 4.09 (s, 3H), 3.70 (t, *J* = 6.6 Hz, 4H), 2.00 (t, *J* = 6.7 Hz, 4H); ^{13}C NMR (125 MHz, $CDCl_3$): δ 25.5, 46.7, 53.5, 111.2, 121.0, 123.6, 124.5, 133.3, 153.5, 157.3, 166.9. HRMS (FAB) m/z calcd for $C_{13}H_{16}N_3O$ $(M+H)^+$: 230.1293, found: 230.1302. *Anal* calcd for $C_{13}H_{15}N_3O$: C, 68.10; H, 6.59; N, 18.33, found: C, 67.95; H, 6.72; N, 18.33.

2-*N*-Azetidino-4-methoxyquinazoline (7d): According to the general procedure the compound was obtained in 74% yield (165 mg) by the reaction of 2-chloro-4-methoxyquinazoline (**6a**) (200 mg, 1.03 mmol), K_2CO_3 (86 mg, 0.62 mmol) and azetidine (125 μL, 2.6 mmol) in dry toluene (15 mL) at 100 °C. Column chromatography (Al_2O_3- Alox(III/N), ethyl acetate/*n*-pentane = 1:20 (v/v)) afforded compound **7d** as solid, mp 124-126 °C; R_f = 0.25 (Al_2O_3, ethyl acetate/*n*-pentane = 1:20 (v/v)). ^{1}H NMR (400 MHz, $CDCl_3$) δ 2.36 ("quint", 2H), 4.07 (s, 3H), 4.23 (t, *J* = 7.5 Hz, 4H), 7.12 (ddd, *J* = 8.0 Hz, *J* = 6.5 Hz, *J* = 1.4 Hz, 1H), 7.54-7.52 (m, 1H), 7.58 (ddd, *J* = 8.2 Hz, *J* = 6.7 Hz, *J* = 1.4 Hz, 1H), 7.91 (d, *J* = 8.0 Hz, 1H); ^{13}C NMR (100 MHz, $CDCl_3$) δ 16.3, 50.3, 53.8, 111.8, 121.7, 123.8, 124.8, 133.6, 153.4, 160.0, 167.6. HRMS (ESI) m/z calcd for $C_{12}H_{14}N_3O$ $(M+H)^+$: 216.1137, found: 216.1138.

2-*N,N*-Dimethylamino-4-methoxyquinazoline (7f): According to the general procedure the compound was obtained in 89% yield (93 mg) by the reaction of 2-chloro-4-methoxyquinazoline (**6a**) (100 mg, 0.51 mmol) with dimethylamine (5.1 mL, 10.2 mmol, 2M in THF) in dry 1,4-dioxane (10 mL) at 100 °C (12h) in a sealed Schlenk tube. Column chromatography (SiO_2, ethyl acetate/*n*-pentane = 1:10 (v/v)) afforded compound **7f** as solid, mp 59-61 °C (colorless needles, *n*-pentane at -28 °C), R_f = 0.64 (SiO_2, ethyl acetate/*n*-pentane = 1:10 (v/v)). ^{1}H NMR (400 MHz, $CDCl_3$): δ 3.27 (s, 6H), 4.09 (s, 3H), 7.09 (ddd, *J* = 8.0 Hz, *J* = 6.6 Hz, *J* = 1.0 Hz, 1H), 7.50 (d, *J* = 8.2 Hz, 1H), 7.57 (ddd, *J* = 8.2 Hz, *J* = 6.6 Hz, *J* = 1.4 Hz, 1H), 7.89 (d, *J* = 8.0 Hz, 1H); ^{13}C NMR (125

MHz, $CDCl_3$): δ 37.2, 53.7, 111.2, 121.3, 123.7, 124.9, 133.5, 153.8, 159.4, 167.1. HRMS (ESI) m/z calcd for $C_{11}H_{14}N_3O$ $(M+H)^+$: 204.1137, found: 204.1141.

2-*N*-Methylamino-4-methoxyquinazoline (7g): According to the general procedure the compound was obtained in 55% yield (40 mg) after column chromatography (SiO_2, *n*-hexane/ethyl acetate = 4:1 (v/v)). Compound **7g** was obtained as solid, mp 127-129 °C; R_f = 0.33 (SiO_2, hexane/ ethyl acetate = 1:1 (v/v)). ^{1}H NMR (300 MHz, $CDCl_3$): δ 3.09 (d, *J* = 5.2 Hz, 3H), 4.07 (s, 3H), 5.05 (bs, 1H), 7.13 (m, 1H), 7.51 (d, *J* = 7.9 Hz, 1H), 7.59 (m, 1H), 7.91 (dd, *J* = 7.6, *J* = 1.7 Hz, 1H); ^{13}C NMR (125 MHz, $CDCl_3$): δ 28.5, 53.8, 112.1, 121.7, 123.7, 124.5, 133.5, 153.0, 159.5, 167.5. HRMS (ESI) m/z calcd for $C_{11}H_{12}N_3O$ $(M+H^+)$: 190.0975; found: 190.1004. *Anal* calcd for $C_{10}H_{11}N_3O$: C, 63.48; H, 5.86; N, 22.21, found: C, 63.23; H, 6.12; N, 22.06.

2-*N*-morpholino-4,5-dimethoxyquinazoline (8a): According to the general procedure the compound was obtained in 84% yield (30 mg) by the reaction of 2-chloro-4,5-dimethoxyquinazoline (**6b**) (29 mg, 0.13 mmol) and morpholine (0.023 mL, 0.26 mmol) in 1,4-dioxane (2 mL) under reflux for 5 h. Column chromatography (SiO_2, *n*-hexane/ethyl acetate = 4:1 (v/v)) afforded compound **8a** as solid, mp 154-155 °C (colorless needles, $CHCl_3$/pentane); R_f = 0.30 (SiO_2, ethyl acetate/*n*-hexane = 1:4 (v/v)). ^{1}H NMR (300 MHz, $CDCl_3$): δ 3.77-3.81 (m, 4H), 3.86-3.90 (m, 4H), 3.93 (s, 3H), 4.07 (s, 3H), 6.56 (d, *J* = 7.5 Hz, 1H), 7.11 (d, *J* = 8.6 Hz, 1H,), 7.47 (dd, *J* = 7.5 Hz, *J* = 8.6 Hz, 1H); ^{13}C NMR (125 MHz, $CDCl_3$): δ 44.4, 54.0, 56.0, 66.9, 102.6, 103.0, 117.8, 133.5, 156.0, 157.6, 158.2, 167.5; HRMS (EI) m/z calcd for $C_{14}H_{17}N_3O_3$ (M^+): 275.1270, found: 275.1262. *Anal* calcd for $C_{14}H_{17}N_3O_3$: C, 61.08; H, 6.22; N, 15.26, found: C, 61.09; H, 6.12; N, 15.15.

4,6-Dimethoxy-2-*N*-morpholinoquinazoline (8b): According to the general procedure the compound was obtained in 62% yield (21 mg) after column chromatography (SiO_2, n-hexane/ethyl acetate = 4:1 (v/v)). Compound **8b** was obtained as colorless solid, mp 152-153 °C (needles, $CHCl_3$/pentane); R_f = 0.27 (SiO_2, ethyl acetate/*n*-hexane = 1/4 (v/v)). ^{1}H NMR (300 MHz, $CDCl_3$): δ 3.78-3.81 (m, 4H), 3.82-3.88 (m, 4H), 3.86 (s, 3H), 4.09 (s, 3H), 7.24-7.30 (m, 2H), 7.46 (d, *J* = 8.9 Hz, 1H); ^{13}C NMR (125 MHz, $CDCl_3$): δ 44.7, 53.7, 55.6, 67.0, 102.1, 111.5, 125.3, 126.6, 148.7, 154.7, 157.6, 166.7; HRMS (EI) m/z calcd for $C_{14}H_{17}N_3O_3$ (M^+): 275.1270, found: 275.1260. *Anal* calcd for $C_{14}H_{17}N_3O_3$: C, 61.08; H, 6.22; N, 15.26, found: C, 61.14; H, 6.16; N, 15.21.

4,7-Dimethoxy-2-*N*-morpholinoquinazoline (8c): According to the general procedure the compound was obtained in 60% yield (441 mg) after column chromatography (SiO_2, *n*-hexane/ethyl acetate = 4:1 (v/v)). Compound **8c** was obtained as solid, mp 143-144 °C (colorless needles, $CHCl_3$/pentane); R_f = 0.36 (SiO_2, ethyl acetate/*n*-hexane = 1:4 (v/v)). ^{1}H NMR (300 MHz, $CDCl_3$): δ 3.78-3.82 (m, 4H), 3.87-3.91 (m, 4H), 3.88 (s, 3H), 4.05 (s, 3H), 6.76 (dd, *J* = 2.4 Hz, *J* = 8.7 Hz, 1H), 6.87 (d, *J* = 2.4 Hz, 1H), 7.79 (d, *J* = 8.7 Hz, 1H); ^{13}C NMR (125 MHz, $CDCl_3$): δ 44.6, 53.5, 55.4, 67.0, 104.1, 105.9, 114.0, 125.0, 155.5, 159.1, 164.1, 167.0; HRMS (EI) m/z calcd for $C_{14}H_{17}N_3O_3$ (M^+): 275.1270, found: 275.1251. *Anal* calcd for $C_{14}H_{17}N_3O_3$: C, 61.08; H, 6.22; N, 15.26, found: C, 60.95; H, 6.09; N, 15.26.

4,8-Dimethoxy-2-*N*-morpholinoquinazoline (8d): According to the general procedure the compound was obtained in 99% yield (437 mg) after column chromatography chromatography (SiO_2, *n*-hexane/ethyl acetate = 4:1 (v/v)). Compound **8d** was obtained as solid, mp 174-175 °C (colorless needles, $CHCl_3$/pentane); R_f = 0.18 (SiO_2, ethyl acetate/*n*-hexane = 1:4 (v/v)). ^{1}H NMR (300 MHz, $CDCl_3$): δ 3.80 (t, *J* = 4.8 Hz, 4H), 3.93 (t, *J* = 4.8 Hz, 4H), 3.98 (s, 3H), 4.09 (s, 3H), 7.00-7.11 (m, 2H), 7.51-7.54 (m, 1H); ^{13}C NMR (125 MHz, $CDCl_3$): δ 44.6, 53.8, 56.1, 67.0, 112.0, 112.3, 115.3, 121.5, 145.0, 152.6, 158.1, 167.4; HRMS (EI) m/z calcd for $C_{14}H_{17}N_3O_3$ (M^+): 275.1270, found: 275.1251. *Anal* calcd for $C_{14}H_{17}N_3O_3$: C, 61.08; H, 6.22; N, 15.26, found: C, 60.98; H, 6.24; N, 15.24.

4,6,7-Trimethoxy-2-*N*-morpholinoquinazoline (10): According to the general procedure the compound was obtained in 98% yield (343 mg) after column chromatography (SiO_2, hexane/ethyl acetate = 4:1(v/v)). Compound **10** was obtained as solid, mp 217-218 °C ($CHCl_3$/*n*-hexane); R_f = 0.09 (SiO_2, ethyl acetate/*n*-hexane = 1:4 (v/v)). ^{1}H NMR (300 MHz, $CDCl_3$): δ 3.80 (t, *J* = 4.8 Hz, 4H), 3.86 (t, *J* = 4.8 Hz, 4H), 3.94 (s, 3H), 3.98 (s, 3H), 4.07 (s, 3H), 7.21 (s, 1H), 7.26 (s, 1H); ^{13}C NMR (125 MHz, $CDCl_3$): δ 44.7, 53.5, 56.0, 56.1, 67.0, 102.1, 104.8, 104.9, 146.2, 150.3, 155.3, 158.3, 166.2. HRMS (FAB) m/z calcd for $C_{15}H_{19}N_3O_4$ $(M+H^+)$: 306.1454, found: 306.1462. *Anal* calcd for $C_{15}H_{19}N_3O_4$: C, 59.01; H, 6.27; N, 13.76, found: C, 59.12; H, 6.35; N, 13.65.

5-Chloro-4-methoxy-2-*N*-morpholinoquinazoline (9a): According to the general procedure the compound was obtained in 86% yield (1159 mg) after column chromatography (SiO_2, *n*-hexane/ethyl acetate = 4:1(v/v)). Compound **9a** was obtained as solid, mp 131-133 °C; R_f = 0.28 (SiO_2, *n*-hexane/ethyl acetate = 4:1 (v/v)). ^{1}H NMR (600 MHz, $CDCl_3$): δ 7.44-7.41 (m, 2H), 7.16 (m, 1H), 4.09 (s, 3H), 3.91 (m, 4H), 3.79 (m, 4H); ^{13}C NMR (150 MHz, $CDCl_3$): δ 44.4, 53.9, 66.9, 109.9, 124.3, 124.7, 130.8, 132.9, 155.7, 157.7, 166.8. HRMS (ESI) m/z calcd for $C_{13}H_{15}ClN_3O_2$ $(M+H^+)$: 280.0847, found: 280.0836. *Anal* calcd for $C_{13}H_{14}ClN_3O_2$: C, 55.82; H, 5.04; N, 15.02, found: C, 55.75; H, 5.09; N, 14.89.

6-Chloro-4-methoxy-2-*N*-morpholinoquinazoline (9b): According to the general procedure the compound was obtained in 89% yield (179 mg) after column chromatography (SiO_2, *n*-hexane/ethyl acetate = 3:1 (v/v)). Compound **9b** was obtained as solid, mp 99-100 °C; R_f = 0.28 (SiO_2, n-hexane/ethyl acetate = 4:1 (v/v)). ^{1}H NMR (600 MHz, $CDCl_3$): δ 7.88 (d, *J* = 2.8 Hz, 1H), 7.53-7.47 (m, 2H), 4.08 (s, 3H), 3.91 (m, 4H), 3.80 (m, 4H); ^{13}C NMR (150 MHz, $CDCl_3$): δ 44.6, 54.0, 66.9, 112.1, 122.9, 126.4, 127.0, 134.2, 151.6, 158.3, 166.6. HRMS (ESI) m/z calcd for $C_{13}H_{15}ClN_3O_2$ $(M+H^+)$: 280.0847, found: 280.0853. *Anal* calcd for $C_{13}H_{14}ClN_3O_2$: C, 55.82; H, 5.04; N, 15.02, found: C, 55.77; H, 5.04; N, 14.91.

7-Chloro-4-methoxy-2-*N*-morpholinoquinazoline (9c): According to the general procedure the compound was obtained in 96% yield (390 mg) after column chromatography (SiO_2, *n*-hexane/ethyl acetate = 9:1 (v/v)). Compound **9c** was obtained as solid, mp 116-117 °C (CH_2Cl_2/*n*-hexane), R_f = 0.33 (SiO_2, ethyl acetate/*n*-hexane = 1:9 (v/v)). ^{1}H NMR (300 MHz, $CDCl_3$): δ 3.77-3.82 (m, 4H), 3.87-3.92 (m, 4H), 4.07 (s, 3H), 7.08 (dd, *J* = 2.0 Hz, *J* = 8.6 Hz, 1H), 7.48 (d, *J* = 2.0 Hz, 1H,), 7.82 (d, *J* = 8.6 Hz, 1H); ^{13}C NMR (125 MHz, $CDCl_3$): δ 44.5, 53.8, 66.9, 110.0, 122.6, 124.2, 125.0, 139.6, 154.1, 158.9, 167.2; HRMS (EI) m/z calcd for $C_{13}H_{14}ClN_3O_2$ (M^+): 279.0775, found: 279.0780. *Anal* calcd for $C_{13}H_{14}ClN_3O_2$: C, 55.82; H, 5.04; N, 15.02, found: C, 55.77; H, 5.06; N, 15.00.

8-Chloro-4-methoxy-2-*N*-morpholinoquinazoline (9d): According to the general procedure the compound was obtained in 82% yield (66 mg, 0.24 mmol) after Column chromatography (SiO_2, *n*-hexane/ethyl acetate = 3:1 (v/v)). Compound **9d** was obtained as a solid, mp 123-124 °C; R_f = 0.35 (SiO_2, *n*-hexane/ethyl acetate = 4:1 (v/v). ^{1}H NMR (500 MHz, $CDCl_3$): δ 7.84 (dd, *J* = 8.1

Hz, 1.4 Hz, 1H), 7.70 (dd, *J* = 7.6 Hz, 1.3 Hz, 1H), 7.05 (t, *J* = 7.8 Hz, 1H), 4.10 (s, 3H), 3.98 (m, 4H), 3.82 (m, 4H); ^{13}C NMR (126 MHz, $CDCl_3$): δ 44.5, 54.1, 66.9, 112.8, 121.4, 122.5, 129.0, 133.5, 149.4, 158.2, 167.6. HRMS (FAB) m/z calcd for $C_{13}H_{15}ClN_3O_2$ ($M+H^+$): 280.0847, found: 280.0834. *Anal* calcd for $C_{13}H_{14}ClN_3O_2$: C, 55.82; H, 5.04; N, 15.02, found: C, 55.92; H, 4.70; N, 14.88.

Synthesis of 2-amino-4-methoxyquinazolines via the Buchwald-Hartwig reaction.

2-*N*-Aziridino-4-methoxyquinazoline (7e): Into a Schlenk tube was added 2-chloro-4-methoxyquinazoline (**6a**) (100 mg, 0.51 mmol), $Pd(OAc)_2$ (3.4 mg, 0.015 mmol), Xantphos (11.6 mg, 0.02 mmol) and Cs_2CO_3 (332 mg, 1.02 mmol). Then, the tube was evacuated and filled with nitrogen and anhydrous toluene (10 mL) and aziridine (53 µL, 1.02 mmol) were added. The mixture was stirred at 100 °C for 3 days. The reaction mixture was filtered through a plug of Celite® and afterwards all volatile solvents were evaporated. Column chromatography (Al_2O_3-Alox(III/N), ethyl acetate/*n*-pentane = 1:10 (v/v)) afforded **7e** (75 mg, 73% yield) as solid, mp 68-70 °C; R_f = 0.39 (Al_2O_3, ethyl acetate/*n*-pentane = 1:10 (v/v)). ^{1}H NMR (400 MHz, $CDCl_3$): δ 2.46 (s, 4H), 4.17 (s, 3H), 7.36 (ddd, *J* = 8.1 Hz, *J* = 5.8 Hz, *J* = 2.2 Hz, 1H), 7.74-7.69 (m, 2 H), 8.03 (d, *J* = 8.1 Hz, 1H); ^{13}C NMR (100 MHz, $CDCl_3$): δ 27.7 (t), 54.4 (q), 114.1 (s), 123.7 (d), 124.8 (d), 126.3 (d), 133.8 (d), 152.2 (s), 166.0 (s), 168.3 (s); HRMS (ESI) m/z calcd for $C_{11}H_{12}N_3O$ ($[M+H]^+$): 202.0980; found: 202.0985.

4-Methoxy-7-nitro-2-*N*-morpholinoquinazoline (11):[57] A mixture of 2-chloro-4-methoxy-7-nitroquinazoline (**6k**) (350 mg, 1.46 mmol), morpholine (0.26 mL, 2.95 mmol) and 1,4-dioxane (15 mL) was heated to reflux for 16 h. Column chromatography (SiO_2, *n*-hexane/ethyl acetate = 4:1 (v/v)) afforded compound **11** (407 mg, 96% yield) as a solid; mp 177-178 °C (yellow needles, $CHCl_3$/pentane). ^{1}H NMR (300 MHz, $CDCl_3$): δ 3.79-3.82 (m, 4H), 3.93-3.96 (m, 4H), 4.12 (s, 3H), 7.84 (dd, *J* = 2.0 Hz, *J* = 8.9 Hz, 1H), 8.02 (d, *J* = 8.9 Hz, 1H), 8.30 (d, *J* = 2.0 Hz, 1H); ^{13}C NMR (125 MHz, $CDCl_3$): δ 44.5, 54.2, 66.9, 114.9, 115.0, 120.5, 125.5, 151.4, 153.4, 159.1, 167.1; HRMS (EI) m/z calcd for $C_{13}H_{14}N_4O_4$ (M^+): 290.1015, found: 290.1002. *Anal* calcd for $C_{13}H_{14}N_4O_4$: C, 53.79; H, 4.86; N, 19.30, found: C, 53.85; H, 4.62; N, 19.23.

4-Methoxy-2-*N*-morpholino-7-aminoquinazoline (12):[58] A 1 *M* aq. HCl solution (0.6 mL) was added to a mixture of compound **11** (58.0 mg, 0.20 mmol) and iron powder (35 mg, 0.60 mmol) in EtOH (10 mL) and kept reflux for 3 h. The mixture was cooled down and filtered. Aqueous ammonium solution was added and the product was extracted with ethyl acetate and washed with brine. After being dried with sodium sulfate, the organic layer was concentrated. Column chromatography (SiO_2, *n*-hexane/ethyl acetate = 1:1 (v/v)) gave compound **12** (44 mg, 85% yield) as solid; mp 205-206 °C; R_f = 0.21 (SiO_2, ethyl acetate/*n*-hexane = 1/1 (v/v)). ^{1}H NMR (300 MHz, $CDCl_3$): δ 3.78 (m, 4H) 3.87 (m, 4H), 4.03 (s, 3H), 4.06 (s, 2H), 6.53 (dd, *J* = 2.1 Hz, *J* = 8.6, 1H), 6.64 (d, *J* = 2.1 Hz, 1H), 7.71 (d, *J* = 8.6 Hz, 1H); ^{13}C NMR (125 MHz, $CDCl_3$): δ 44.6, 53.3, 67.0, 104.4, 105.7, 112.7, 125.2, 151.3, 155.0 159.0, 166.9. HRMS (EI) m/z calcd for $C_{13}H_{16}N_4O_2$ (M^+): 260.1273, found: 260.1243. *Anal* calcd for $C_{13}H_{16}N_4O_2$: C, 59.99; H, 6.20; N, 21.52, found: C, 59.74; H, 5.93; N, 21.23.

Supporting information

Additional experimental procedures, analytical and spectroscopic data including UV-vis absorption and PLE spectra in solution and solid state, cyclic voltammetry data, thermogravimetric analyses (TGA), crystallographic data (CCDC 2081759, 2081760 and 2081761) molecular orbitals, Cartesian coordinates of optimized ground states, excitation energies for the excited states 1-5, and orbital transition assignment and oscillator strengths for selected compounds are provided in the supplementary information.

Acknowledgements

Financial support of the Ministère de l'Enseignement Supérieur et de la Recherche (MESR), the Centre National de la Recherche Scientifique (CNRS, France) and the Conseil Régional de Normandie and the Fonds Européen de Développement Régional (FEDER) is gratefully acknowledged.

Keywords: fluorescence spectroscopy • quinazolines • cyclic voltammetry • push-pull chromophores • intramolecular charge transfer (ICT) • HOMO/LUMO • fluorescence-structure-property relationship (FSPR)

[1] (a) N. Kerru, L. Gummidi, S. Maddila, K. K. Gangu, S. B. Jonnalagadda, *Molecules* **2020**, *25*, 1909-1951; (b) V. Alagarsamy, K. Chitra, G. Saravanan, V. R. Solomon, M. T. Sulthana, B. Narendhar, *Eur. J. Med. Chem*. **2018**, *151*, 628-685; (c) A. Hameed, M. Al-Rashida, M. Uroos, S. A. Ali, A. M. Ishtiaq, K. M. Khan, *Expert Opin. Ther. Pat*. **2018**, *28*, 281-297; (d) I. Khan, S. Zaib, S. Batool, N. Abbas, Z. Ashraf, J. Iqbal, A. Saeed, *Bioorg. Med. Chem*. **2016**, *24*, 2361-2381; (e) G. N. Lipunova, E. V. Nosova, V. N. Charushin, O. N. Chupakhin, *Russ. Chem. Rev*. **2016**, *85*, 759-793; (f) I. Khan, A. Ibrar, N. Abbas, A. Saeed, *Eur. J. Med. Chem.* **2014**, *76*, 193-244.

[2] G. N. Lipunova, E. V. Nosova, V. N. Charushin, O. N. Chupakhin, *Current Org. Synth*. **2018**, *15*, 793-814.

[3] A. M. Alafeefy, A. A. Kadi, O. A. Al-Deep, K. E. El-Tahir, N. A. Al-Jaber, *Eur. J. Med. Chem*. **2010**, *45*, 4947-4952.

[4] K. Waisser, J. Gregor, H. Dostal, J. Kunes, L. Kubicova, V. Klimesova, J. Kaustova, *It. Farmaco* **2001**, *56*, 803-807.

[5] (a) F. E. Held, A. A. Guryev, T. Fröhlich, F. Hampel, A. Kahnt, C. Hutterer, M. Steingruber, H. Bahsi, C. von Bojnicic-Kninski, D. S. Mattes, T. C. Foertsch, A. Nesterov-Mueller, M. Marschall, S. B. Tsogoeva, *Nat. Commun*. **2017**, *8*, 15071-15079; (b) C. Hutterer, S. T. Hamilton, M. Steingruber, I. Zeittrager, H. Bahsi, N. Thuma, Z. Orfi, L. Orfi, E. Socher, H. Sticht, W. D. Rawlinson, S. Chou, V. J. Haupt, M. Marschall, *Antiviral Res*. **2016**, *134*, 130-143; (c) Z. Wan, D. Hu, P. Li, D. Xie, X. Gan, *Molecules* **2015**, *20*, 11861-11874.

[6] (a) M. H. Bule, I. Ahmed, F. Maqbool, M. A. Zia, *Int. J. Pharmacol*. **2017**, *13*, 818-831; (b) S. Madapa, Z. Tusi, A. Mishra, K. Srivastava, S. K. Pandey, R. Tripathi, S. K. Puri, S. Batra, *Bioorg. Med. Chem*. **2009**, *17*, 222-234.

[7] A. Reza, J. M. Sutton, K. M. Rahman, *Antibiotics* **2019**, *8*, 229-248.

[8] F. Liu, Y. J. Huang, *Pestic. Biochem. Physiol*. **2011**, *101*, 248-255.

[9] M. Cakici, M. Catir, S. Karabuga, H. Kilic, S. Ulukanli, M. Gulluce, F. Orhan, *Tetrahedron: Asymmetry* **2010**, *21*, 2027-2031.

[10] K. S. Van Horn, X. Zhu, T. Pandharkar, S. Yang, B. Vesely, M. Vanaerschot, J.-C. Dujardin, S. Rijal, D. E. Kyle, M. Z. Wang, K. A. Werbovetz, R. Manetsch, *J. Med. Chem*. **2014**, *57*, 5141-5136.

[11] S. Sasmal, G. Balaji, H. R. K. Reddy, D. Balasubrahmanyam, G. Srinivas, S. Kyasa, P. K. Sasmal, I. Khanna, R. Talwar, J. Suresh, V. P. Jadhav, S. Muzeeb, D. Shashikumar, K. H. Reddy, V. J. Sebastian, T. M. Frimurer, Ø. Rist, L. Elster, T. Högberg, *Bioorg. Med. Chem. Lett*. **2012**, *22*, 3157-3162.

[12] (a) Shagufta, I. Ahmad, *Med. Chem. Comm*. **2017**, *8*, 871-885; (b) Y. Suzuki, A. Otake, S. Ueno, K. Hayahi, H. Ishii, N. Miyoshi, K. Kuroiwa, M. Tachikawa, Y. Fujimaki, K. Nishiyama, K. Manabe, R. Yamazaki, A. Asai, *ACS Med. Chem. Lett*. **2018**, *11*, 1287-1291; (c) Y. Zhang, Q. Hou, X. Li, J. Zhu, W. Wang, B. Li, L. Zhao, H. Xia, *Eur. J. Med. Chem*. **2019**, *178*, 417-432; (d) M. K. Krapf, M. Wiese, *J. Med. Chem*. **2016**, *59*, 5449-5461; (e) S. Ravez, O. Castillo-Aguilera, P. Depreux, L. Goossens, *Expert Opin. Ther. Pat*. **2015**, *25*, 789-804; (f) K. Kuroiwa, H. Ishii, K. Matsuno, A. Asai, Y. Suzuki, *ACS Med. Chem. Lett*. **2015**, *6*, 287-291; (g) Y. Zhang, L. Jin H. Xiang, J. Wu, P. Wang, D. Hu, W. Xue, S. Yang, *Eur. J. Med. Chem*. **2013**, *66*, 335-344.

[13] F. Shan, Z. Shao, S. Jiang, Z. Cheng, *Cancer Med*. **2016**, *5*, 3166-3175.

[14] T. P. Selvam, P. V. Kumar, *Research in Pharmacy* **2011**, *1*, 1-21.

[15] A. Desiniotis, N. Kyprianou, *Expert Opin. Ther. Targets* **2011**, *15*, 1405-1418.

[16] P. A. Corral, J. F. Botello, C. Xing, *Bioorg. Med. Chem. Lett*. **2020**, *30*, 126719-126723.

[17] (a) G. Le-Nhat-Thuy, N. N. Thi, H. Pham-The, T. A. D. Thi, H. N. Thi, T. H. N. Thi, S. N. Hoang, T. V. Nguyen, *Bioorg. Med. Chem. Lett*. **2020**, *30*, 127404; (b) N. Q. Thai, Z. Bednarikova, M. Gancar, H. Q. Linh, C.-K. Hu, M. S. Li, Z. Gazova, *ACS Chem. Neurosci*. **2018**, *9*, 2588-2598; (c) T. Mohamed, P. P. N. Rao*, Eur. J. Med. Chem*. **2017**, *126*, 823-843.

[18] H. S. Haniff, Y. Tong, X. Liu, J. L. Chen, B. M. Suresh, R. J. Andrews, J. M. Peterson, C. A. O'Leary, R. I. Benhamou, W. N. Moss, M. D. Disney, *ACS Cent. Sci*. **2020**, *6*, 1713-1721.

[19] (a) S. Achelle, J. Rodriguez-Lopez, F. Robin-le Guen, *J. Org. Chem.* **2014**, *79*, 7564-7571; (b) J. Yuan, Y. Yuan, X. Tian, Y. Liu, J. Sun, *J. Phys. Chem. C* **2017**, *121*, 8091-8108.

[20] (a) B. Li, X. Song, X. Jiang, Z. Li, F. Guo, Y. Wang, L. Zhao, Y. Zhang, *Chin. Chem. Lett*. **2020**, *31*, 1188-1192; (b) S. M. Kim, J. H. Yun, S. H. Han, J. Y. Lee, *J. Mater. Chem. C* **2017**, *5*, 9072-9079; (c) D. Y. Kim, J. Kang, S. E. Lee, Y. K. Kim, S. S. Yoon, *Luminescence* **2017**, *32*, 1180-1185; (d) Z. Zhang, J. Xie, H. Wang, B. Shen, J. Zhang, J. Hao, J. Cao, Z. Wang, *Dyes and Pigments* **2016**, *125*, 299-308.

[21] R. Keruckiene, S. Vekteryt, E. Urbonas, M. Guzauskas, E. Skuodis, D. Volyniuk, J. V. Grazulevicius, *Beilstein J. Org. Chem*. **2020**, *16*, 1142-1153.

[22] (a) B. Li, Z. Li, F. Guo, J. Song, X. Jiang, Y. Wang, S. Gao, J. Wang, X. Pang, L. Zhao, Y. Zhang, *ACS Appl. Mater. Interfaces* **2020**, *12*, 14233-14243; (b) D. Liu, Z. Zhang, H. Zhang, Y. Wang, *Chem. Commun*. **2013**, *49*, 10001-10003; (c) N. A. Kukhta, M. R. Bryce, *Mater. Horiz*. **2021**, *8*, 33-55.

[23] (a) K. Aoki, R. Osako, J. Deng, T. Hayashita, T. Hashimoto, Y. Suzuki, *RSC Adv.* **2020**, *10*, 15299-15306; (b) J. Kimura, H. Yamada, H. Ogura, T. Yajima, T. Fukushima*, Anal. Chim. Acta* **2009**, *635*, 207-213.

[24] M. Mao, X. Zhang, B. Zhu, J. Wang, G. Wu, Y. Yin, Q. Song, *Dyes and Pigments* **2016**, *124*, 72-81.

[25] (a) Q. Mei, J. Weng, Z. Xu, B. Tong, Q. Hua, Y. Shi, J. Song, W. Huang, *RSC Adv*. **2015**, *5*, 97841-97848; (b) Q. Mei, L. Wang, Y. Guo, J. Weng, F. Yan, B. Tian, B. Tong, *J. Mater. Chem. C* **2012**, *22*, 6878-6884.

[26] B. Li, Z. Wang, S.-J. Su, F. Guo, Y. Cao, Y. Zhang, *Adv. Optical Mater*. **2019**, 1801496.

[27] (a) G. V. Baryshnikov, P. Gawrys, K. Ivaniuk, B. Witulski, R. J. Whitby, A. Al-Muhammad, B. Minaev, V. Cherpak, P. Stakhira, D. Volyniuk, G. Wiosna-Salyga, B. Luszczynska, A. Lazauskas, S. Tamulevicius, J. V. Grazulevicius, *J. Mater. Chem. C* **2016**, *4*, 5795-5805; (b) K. T. Kamtekar, A. P. Monkman, M. R. Bryce, *Adv. Mater*. **2010**, *22*, 572-582.

[28] (a) M. J. Mphahlele, H. K. Paumo, L. Rhyman, P. Ramasami, *Molecules* **2015**, *20*, 14656-14683; (b) M. J. Mphahlele, H. K. Paumo, A. M. El-Nahas, M. M. El-Hendawy, *Molecules* **2014**, *19*, 795-818.

[29] J. Dhuguru, W. Liu, W. G. Gonzalez, W. M. Babinchak, J. Miksovska, R. Landgraf, J. N. Wilson, *J. Org. Chem*. **2014**, *79*, 4940−4947.

[30] (a) E. V. Nosova, T. N. Moshkina, G. N. Lipunova, D. S. Kopchuk, P. A. Slepukhin, I. V. Baklanova, V. N. Charushin, *Eur. J. Org. Chem*. **2016**, 2876-2881; (b) M. Wang, G. Zhang, Y. Wang, J. Wang, M. Zhu, S. Chen, Y. Wang, *Bioorg. Med. Chem. Lett.* **2020**, *30*, 127143; (c) H. P. Lakum, D. R. Shah, K. H. Chikhalia, *J. Heterocyclic Chem.* **2016**, *53*, 209-219.

[31] Y. Suzuki, J. Sawada, P. Hibner, H. Ishii, K. Matsuno, M. Sato, B. Witulski, A. Asai, *Dyes and Pigm*ents **2017**, *145*, 233-238.

[32] (a) M. Faisal, A. Saeed, *Front. Chem.* **2021**, *8*, 594717; (b) P. S. Auti, G. George, A. T. Paul, *RSC Adv.* **2020**, *10*, 41353-41392; (c) I. Khan, A. Ibrar, W. Ahmed, A. Saeed, *Eur. J. Med. Chem.* **2015**, *90*, 124-169; (d) I. Khan, A. Ibrar, N. Abbas, A. Saeed, *Eur. J. Med. Chem.* **2014**, *76*, 193-244.

[33] (a) S. Pal, B. Paul, P. Bandopadhyay, N. Preethy, D. Sarkar, O. Rahman, S. Goon, S. Roy, D. Ganguly, A. Talukdar, *Eur. J. Med. Chem.* **2021**, *210*, 112978; (b) A. Castán, R. Badorrey, J. A. Díez, C. T. Christoffersen, L. K. Rasmussen, J. Kehler, R. Köhler, J. A. Gálvez, M. D. Díaz-de-Villegas, *J. Org. Chem*. **2020**, *85*, 5941–5951; (c) R. A. Smits, I. J. P. de Esch, O. P. Zuiderveld, J. Broeker, K. Sansuk, E. Guaita, G. Coruzzi, M. Adami, E. Haaksma, R. Leurs, *J. Med. Chem.* **2008**, *51*, 7855-7865; (d) S. T. Henriksen, U. S. Sørensen, *Tetrahedron Lett.* **2006**, *47*, 8251-8254.

[34] T. Kanzian, T. A. Nigst, A. Maier S. Pichl, H. Mayr, *Eur. J. Org. Chem.* **2009**, 6379-6385.

[35] P. Ruiz-Castillo, S. L. Buchwald, *Chem. Rev*. **2016**, *116*, 12564-12649.

[36] (a) B. Witulski, S. Senft, J. Bonet, O. Jost, *Synthesis* **2007**, 243-250; (b) B. Witulski, Y. Zimmermann, V. Darcos, J.-P. Desvergne, D. M. Bassani, H. Bouas-Laurent, *Tetrahedron Lett.* **1998**, 39, 4807.

[37] K. Suzuki, A. Kobayashi, S. Kaneko, K. Takehira, T. Yoshihara, H. Ishida, Y. Shiina, S. Oishi, S. Tobita, *Phys. Chem. Chem. Phys.* **2009**, *11*, 9850-9860.

[38] C. Hansch, A. Leo, R. W. Taft, *Chem. Rev.* **1991**, *91*, 165-195.

[39] For related selected correlations of the Hammett substituent constant with UV-vis and PLE properties, see: (a) J. Papadopoulos, T. J.J. Mueller, *Dyes and Pigments* **2019**, *166*, 357-366; (b) M. Ahn, M.-J. Kim, K.-R. Wee, *J. Org. Chem.* **2019**, *84*, 12050-12057; (c) J. V. Jun, E. J. Petersson, D. M. Chenoweth, *J. Am. Chem. Soc.* **2018**, *140*, 9486-9493; (d) J. B. Grimm, A. K. Muthusamy, Y. Liang, T. A. Brown, W. C. Lemon, R. Patel, R. Lu, J. J. Macklin, P. J. Keller, N. Ji, L. D. Lavis, *Nature Methods* **2017**, *14*, 987-994; (e) S. Abou-Hatab, V. A. Spata, S. Matsika, *J. Phys. Chem. A* **2017**, *121*, 1213-1222; (f) J. Shaya, F. Fontaine-Vive, B. Y. Michel, A. Burger, *Chem. Eur. J.* **2016**, *22*, 10627-10637, and ref. cited therein.

[40] C. Reichardt, T. Welton, Solvents and Solvent Effects in Organic Chemistry, 4th edition, Wiley-VCH, Weinheim **2010**.

[41] Z. Zhao, H. Zhang, J. W. Y. Lam, B. Z. Tang, *Angew. Chem.* **2020**, *132*, 9972-9993; *Angew. Chem. In. Ed*. **2020**, *59*, 9888-9907.

[42] H. Srour, T.-H. Doan, E. Da Silva, R. J. Whitby, B. Witulski, *J. Mater. Chem. C* **2016**, *4*, 6270-6279.

[43] N. G. Connelly, W. E. Geiger, *Chem. Rev*. **1996**, *96*, 877-910.

[44] C. M. Cardona, W. Li, A. E. Kaifer, D. Stockdale, G. C. Bazan, *Adv. Mater*. **2011**, *23*, 2367-2371.

[45] (a) M. Cossi, V. Barone, R. Cammi, J. Tomasi, *Chem. Phys. Lett.* **1996**, *255*, 327-335; (b) V. Barone, M. Cossi, J. Tomasi, *J. Chem. Phys.* **1997**, *107*, 3210-3221.

[46] (a) A. D. Becke, *J. Chem. Phys.* **1993**, *98*, 5648−5652; (b) C. Lee, W. Yang, R. G. Parr, *Phys. Rev. B: Condens. Matter Mater. Phys.* **1998**, *37*, 785-789.

[47] Y. Zhao, D. G. Truhlar, *Theor. Chem. Acc.* **2008**, *120*, 215-241.

[48] H. Nakatsuji, K. Hirao, *J. Chem. Phys.* **1978**, *68*, 2053-2065.

[49] R. Bauernschmitt, R. Ahlrichs, *Chem. Phys. Lett.* **1996**, *256*, 454-464.

[50] Gaussian 16, Revision C. 01, M. J. Frisch, G. W. Trucks, H. B. Schlegel, G. E. Scuseria, M. A. Robb, J. R. Cheeseman, G. Scalmani, V. Barone, G. A. Petersson, H. Nakatsuji, X. Li, M. Caricato, A. V. Marenich, J. Bloino, B. G. Janesko, R. Gomperts, B. Mennucci, H. P. Hratchian, J. V. Ortiz, A. F. Izmaylov, J. L. Sonnenberg, D. Williams-Young, F. Ding, F. Lipparini, F. Egidi, J. Goings, B. Peng, A. Petrone, T. Henderson, D. Ranasinghe, V. G. Zakrzewski, J. Gao, N. Rega, G. Zheng, W. Liang, M. Hada, M. Ehara, K. Toyota, R. Fukuda, J. Hasegawa, M. Ishida, T. Nakajima, Y. Honda, O. Kitao, H. Nakai, T. Vreven, K. Throssell, J. A. Montgomery, Jr., J. E. Peralta, F. Ogliaro, M. J. Bearpark, J. J. Heyd, E. N. Brothers, K. N. Kudin, V. N. Staroverov, T. A. Keith, R. Kobayashi, J. Normand, K. Raghavachari, A. P. Rendell, J. C. Burant, S. S. Iyengar, J. Tomasi, M. Cossi, J. M. Millam, M. Klene, C. Adamo, R. Cammi, J. W. Ochterski, R. L. Martin, K. Morokuma, O. Farkas, J. B. Foresman, D. J. Fox, Gaussian, Inc., Wallingford CT, **2016**.

[51] (a) R. A. Kendall, T. H. Dunning, R. J. Harrison, *J. Chem. Phys.* **1989**, *90*, 1007-1023; (b) R. A. Kendall, T. H. Dunning, R. J. Harrison, *J. Chem. Phys.* **1992**, *96*, 6796-6806.

[52] Computational time for compound **2** at SAC-CI level/aug-cc-pVDZ by Intel Xeon Gold 6230 CPU with 348GB memory-ram and 1TB scratch-disk was about 3 days and 4 hours.

[53] J.-L. Bredas, *Mater. Horiz.* **2014**, *1*, 17-19.

[54] (a) M. Nakata, T. Shimazaki, *J. Chem. Inf. Model.* **2017**, *57*, 1300-1308; (b) Y. Abdullayev, A. Mammadov, N. Karimova, A. Talybov, U. Yolchuyeva, J. Autschbach, *ChemistrySelect* **2020**, *5*, 6224-6229.

[55] (a) V. Amendola, L. Fabbrizzi, C. Mangano, P. Pallavicini, *Acc. Chem. Res.* **2001**, *34*, 488-493; (b) A. P. de Silva, H. Q. N. Gunaratne, T. Gunnlaugsson, A. J. M. Huxley, C. P. McCoy, J. T. Rademacher, T. E. Rice, *Chem. Rev*. **1997**, *97*, 1515-1566.

[56] K. S. Van Horn, W. N. Burda, R. Fleeman, L. N. Shaw, R. Manetsch, *J. Med. Chem.* **2014,** *57*, 3075-3093.

[57] J. T. Heppell, J. M. A. Al-Rawi, *J. Heterocyclic Chem.* **2014**, *51*, 162-174.

[58] J. T. Heppell, J. M. A. Al-Rawi, *Med. Chem. Res.* **2016**, *25*, 1695-1704.

10.1002/asia.202100534

WILEY-VCH

FULL PAPER

Entry for the Table of Contents

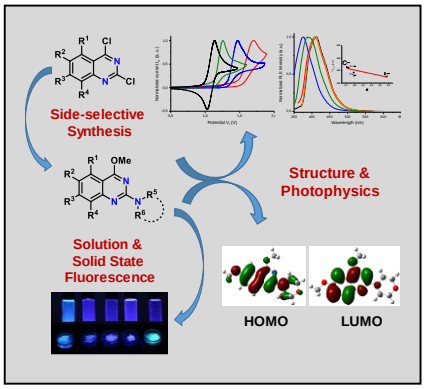

Side-selective synthesis provides sets of new fluorescent 2-*N*-aminoquinazolines whose fluorescent-structure-property relationships (FSPRs) were revealed by steady-state absorption and light emission spectroscopy, electrochemical and computational (DFT-TDDFT/BLYP3 and SAC-CI calculations) chemistry.